AGU PUBLICATIONS

Tectonics

RESEARCH ARTICLE
10.1002/2015TC004091

**Key Points:**
- Spatial distribution of major earthquakes over 1400 years is not random
- Coulomb stress changes control the sequence of major earthquakes
- Several faults capable of Mw ≥ 7 earthquakes may be close to failure

**Supporting Information:**
- Supporting Information S1
- Data Set S1
- Data Set S2
- Data Set S3
- Figure S1
- Figure S2
- Figure S3
- Figure S4
- Figure S5
- Figure S6
- Figure S7
- Figure S8

**Correspondence to:**
A. Verdecchia,
verdecchia.ale@gmail.com

**Citation:**
Verdecchia, A., and S. Carena (2016), Coulomb stress evolution in a diffuse plate boundary: 1400 years of earthquakes in eastern California and western Nevada, USA, *Tectonics*, *35*, 1793–1811, doi:10.1002/2015TC004091.

Received 26 NOV 2015
Accepted 7 JUL 2016
Accepted article online 19 JUL 2016
Published online 8 AUG 2016



# Coulomb stress evolution in a diffuse plate boundary: 1400 years of earthquakes in eastern California and western Nevada, USA

**Alessandro Verdecchia[1] and Sara Carena[1]**

[1]Department of Earth and Environmental Sciences, Ludwig-Maximilians University, Munich, Germany

**Abstract** Diffuse plate boundaries are characterized by deformation distributed over a wide area in a complex network of active faults and by relatively low strain rates. These characteristics make it difficult to understand the spatial and temporal distribution of seismicity. The area east of the Sierra Nevada, between longitudes 121°W and 116°W, is part of a diffuse plate boundary. At least 17 major surface-rupturing earthquakes have happened here in the last 1400 years. Our purpose is to determine whether these events influence each other or whether they are randomly distributed in time and space. We model the evolution of coseismic and postseismic Coulomb failure stress changes (ΔCFS) produced by these earthquakes, and we also model interseismic stresses on the entire fault network. Our results show that 80% of the earthquake ruptures are located in areas of combined coseismic and postseismic ΔCFS ≥ 0.2 bar. This relationship is robust, as shown by the control tests that we carried out using random earthquake sequences. We also show that the Fish Lake Valley, Pyramid Lake, and Honey Lake faults have accumulated 45, 37, and 27 bars, respectively, of total ΔCFS (i.e., coseismic + postseismic + interseismic) in the last 1400 years. Such values are comparable to the average stress drop in a major earthquake, and these three faults may be therefore close to failure.

## 1. Introduction

Most plate boundaries are characterized by high deformation rates localized along a narrow zone, where major earthquakes ($M_w \geq 7$) tend to occur periodically at expected locations on a major plate boundary fault (e.g., San Andreas fault, North Anatolian fault, and megathrusts in subduction zones) [*Stein and Liu*, 2009]. In diffuse plate boundaries, deformation is distributed across wider regions and accommodated by several fault systems with variable slip rates [*Thatcher*, 1995; *Bennett et al*., 2003]. As a consequence, earthquakes in diffuse plate boundaries occur in spatially and temporally complex patterns.

A good example of a diffuse plate boundary is the region east of the Sierra Nevada that encompasses the Eastern California Shear Zone (ECSZ), the Walker Lane, and the westernmost part of the Basin and Range province (Figure 1). Here at least one fifth of the ~ 50 mm/yr of right-lateral transform motion between the Pacific and North America plates is accommodated along a northwest trending zone characterized by a combination of right-lateral strike-slip faults and normal faults [*Bennett et al*., 2003; *DeMets et al*., 2010; *Wesnousky et al*., 2012]. In this study we focus on the area north of the Garlock fault and east of the Sierra Nevada, which includes the ECSZ, the Walker Lane, and the western Basin and Range (Figures 1 and 2). Six major earthquakes ($M_w \geq 7$) have occurred in this region in historical times, and at least another 11 surface-rupturing events that occurred in the last 1400 years have been recognized by paleoseismological studies (Figure 2).

Several authors showed that large earthquakes in this region interact in terms of Coulomb stress. *Hodgkinson et al*. [1996] and *Caskey and Wesnousky* [1997] found that each event in the 1954 Rainbow Mountain-Fairview Peak-Dixie Valley earthquake sequence precipitated the next one by positive coseismic static stress changes. *McAuliffe et al*. [2013] noted the similarity in ages between the most recent events on the Garlock and Panamint Valley faults and proposed Coulomb stress interaction between these two faults as a reason. *Verdecchia and Carena* [2015] found that the 1872 $M_w$ 7.5 Owens Valley earthquake strongly influenced the distribution of subsequent seismicity in the northern ECSZ.

All these previous studies, however, are restricted either to earthquakes that are part of the same spatiotemporal seismic cluster [*Hodgkinson et al*., 1996; *Caskey and Wesnousky*, 1997] or to short periods of time (0 to 150 years) [*McAuliffe et al*., 2013; *Verdecchia and Carena*, 2015]. The limited time range of recorded

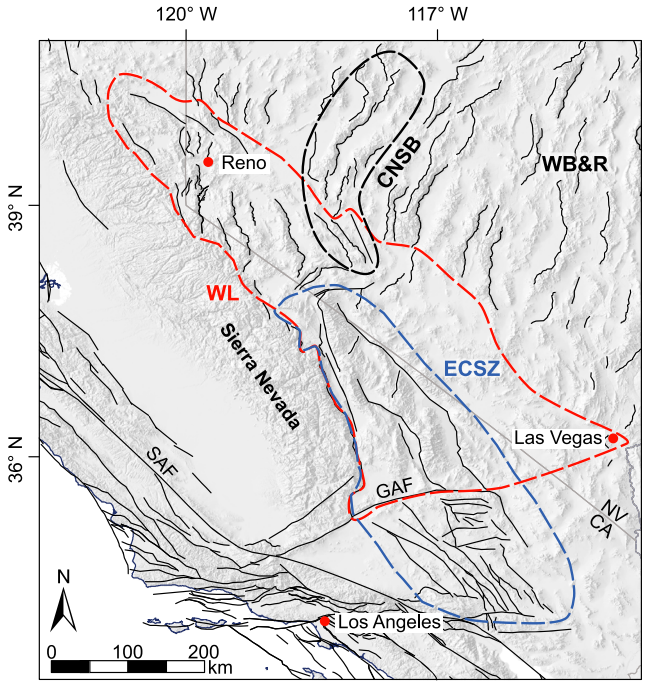


**Figure 1.** Map of active faults in California and central Nevada, from the U.S. Geological Survey National Seismic Hazard Maps [*Petersen et al.*, 2014]. CNSB = Central Nevada Seismic Belt; ECSZ = Eastern California Shear Zone [*Dokka and Travis*, 1990]; WL = Walker Lane [*Stewart*, 1988]; WB&R = western Basin and Range; SAF = San Andreas fault; GAF = Garlock fault.

historical events makes the reconstruction and the interpretation of the evolution of seismicity patterns in the region challenging. In fact, no regional migration patterns have so far been recognized [*Wallace*, 1987], but no systematic study of major faults in the region has been conducted either.

In order to address these issues, we model the coseismic and postseismic Coulomb failure stress changes (ΔCFS) due to 17 ground-rupturing earthquakes in the last 1400 years. We also carry out tests to verify whether the results of our models are better than a random distribution. As a last step, in order to identify likely future sources of major earthquakes, we calculate the total (coseismic + postseismic + interseismic) Coulomb failure stress ($\Delta CFS_{tot}$) accumulated by major faults that produced no large events in the last 1400 years. We show that the distribution of earthquakes throughout the entire region is in fact not random, but rather earthquakes tend to occur in areas of positive cumulative (coseismic + postseismic) Coulomb stress ($\Delta CFS_{cum}$).

## 2. Earthquakes and Faults

We analyze earthquake interactions in this region over the past 1400 years because, unlike the San Andreas fault, where high deformation rates suggest recurrence intervals for large earthquakes of 100 to 300 years [*Field et al.*, 2013], most major faults in our study region rupture at intervals ≥ 1000 years [*Dixon et al.*, 2003].

Due to the fact that earthquakes recognized by paleoseismological methods are ground-rupturing, and therefore start at about $M_w = 7$, we do not consider events smaller than $M_w = 6.5$. Smaller events have anyway a limited effect in terms of areal extent and magnitude of stress changes.

In the next sections we present the data used to model the faults responsible for all the earthquakes used in this study. We consider only the most recent event for each fault except for the Fish Lake Valley Fault. For the latter we model also the penultimate event because these two events occurred on two separate segments of the fault. Each named earthquake below is accompanied by the acronym of its source fault to facilitate identification in the figures and tables.

### 2.1. Historical and Instrumental Earthquakes (1872 A.D. to Present) and Their Source Faults

The 1872 $M_w$ 7.5 Owens Valley earthquake (OVF) [*Beanland and Clark*, 1994] and the 1915 $M_w$ 7.5 Pleasant Valley earthquake (PSF) [*Wallace*, 1984] are the two oldest major historical events in the region. They also mark the southern and northern limits of a ~500 km long right-lateral transtensional zone where several major ground-rupturing earthquakes happened in the last 150 years (Figure 2).

The 1872 Owens Valley earthquake (OVF) created a ~110 km long rupture with right-lateral displacements up to 7 m [*Beanland and Clark*, 1994; *Haddon et al.*, 2016], whereas the 1915 Pleasant Valley earthquake (PSF) was a normal-slip event with little strike-slip motion forming coseismic fault scarps up to 5.8 m high [*Wallace*, 1984]. The latter was followed 17 years later by the 1932 $M_w$ 7.2 Cedar Mountain earthquake (CMF)

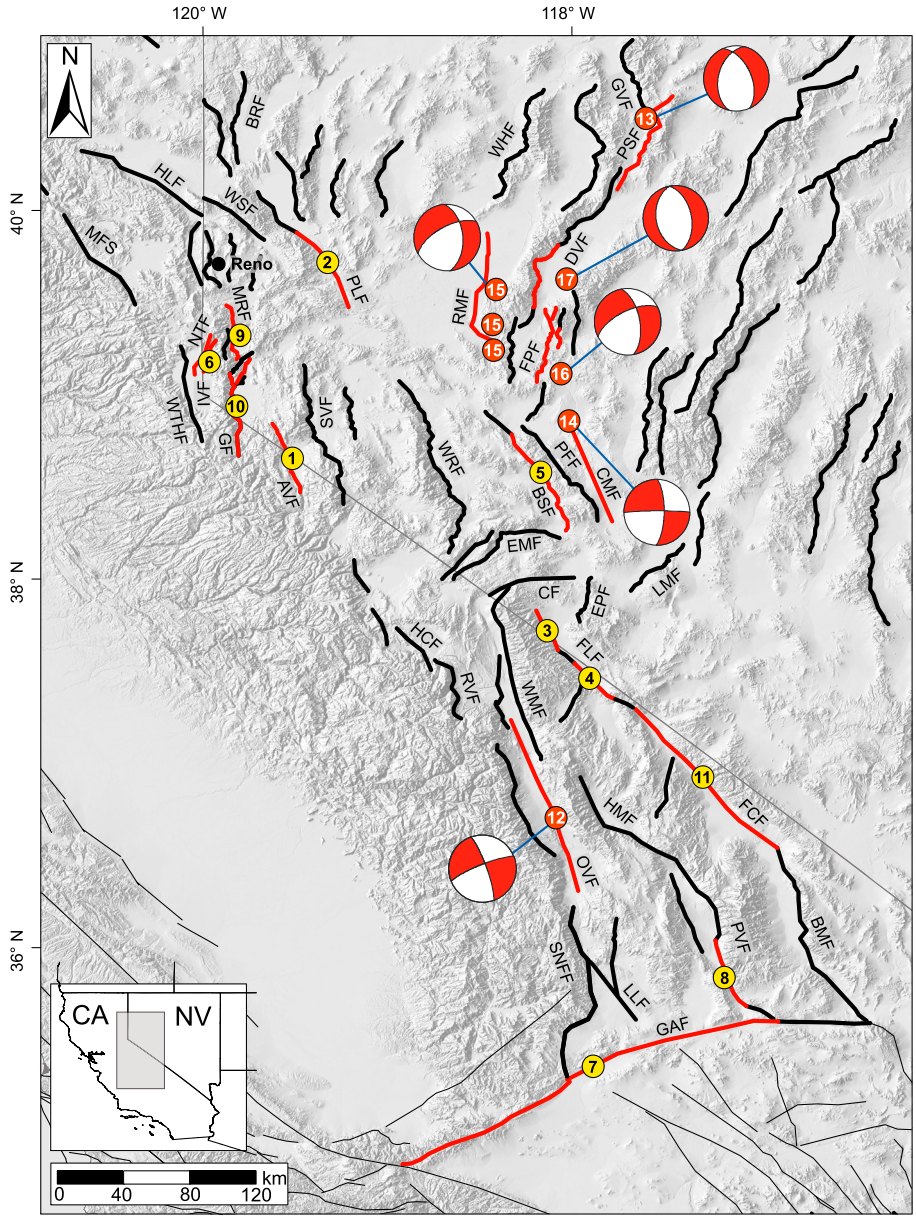


**Figure 2.** Map of Quaternary active faults capable of $M \geq 7$ earthquakes, from the U.S. Geological Survey National Seismic Hazard Maps [*Petersen et al.*, 2014]. Thick red lines represent faults that have produced a surface rupture event in the last 1400 years and thick black lines the rest of the faults modeled in this work. Numbered red and yellow circles represent the sequence of historical and paleoseismological earthquakes, respectively (listed in Table 1). For historical earthquakes, the red circle represents also the specific earthquake epicenter location from the CDMG Historical Earthquakes database [*Petersen et al.*, 1996]. Focal mechanisms are from *Beanland and Clark* [1994] (Owens Valley earthquake), *Doser* [1988] (Pleasant Valley and Cedar Valley earthquakes), and *Doser* [1986] (Rainbow Mountain, Fairview Peak and Dixie Valley earthquakes). AVF = Antelope Valley Fault; BMF = Black Mountains Fault; BSF = Benton Springs Fault; BRF = Bonham Range Fault; CF = Coaldale Fault; CMF = Cedar Mountain Fault; DVF = Dixie Valley Fault; EMF = Excelsior Mountains Fault; EPF = Emigrant Peak Fault; FPF = Fairview Peak Fault; FLF = Fish Lake Fault; FCF = Furnace Creek Fault; GAF = Garlock Fault; GF = Genoa Fault; GVF = Grass Valley Fault; HCF = Hilton Creek Fault; HLF = Honey Lake Fault; HMF = Hunter Mountain Fault; IVF = Incline Village Fault; LLF = Little Lake fault; LMF = Lone Mountain Fault; MFS = Mohawk Fault system; MRF = Mount Rose Fault; NTF = North Tahoe Fault; OVF = Owens Valley Fault; PFF = Petrified Springs Fault; PLF = Pyramid Lake Fault; PSF = Pleasant Valley Fault; PVF = Panamint Valley Fault; RMF = Rainbow Mountain Fault; RVF = Round Valley Fault; SNFF = Sierra Nevada frontal Fault; SVF = Smith Valley Fault; WHF = West Humboldt Fault; WMF = White Mountains Fault; WRF = Wassuk Range Fault; WSF = Warm Springs Fault; WTHF = West Tahoe Fault.

**Table 1.** ΔCFS Immediately Before the Occurrence of Each Earthquake[a]

| | | | | Coseismic ΔCFS (Bars) | Cumulative ΔCFS (Bars) | | | | |
|---|---|---|---|---|---|---|---|---|---|
| | | | | | Model 3 | | | Model 1 | Model 2 |
| | Earthquake[b] (A.D.) | $M_w$ | Strike/Dip/Rake (deg)[c] | $\mu'$ 0.4 | $\mu'$ 0.2 | $\mu'$ 0.4 | $\mu'$ 0.8 | $\mu'$ 0.4 | $\mu'$ 0.4 |
| 1 | 587 AVF | 7.2 | 344/60/−90 | / | / | / | / | / | / |
| 2 | 700 PLF | 7.0 | 340/85/180 | 0.06 | 0.19 | 0.24 | 0.35 | 0.29 | 0.27 |
| 3 | 913 FLFa | 6.8 | 340/80/180 | 0.0 | 0.08 | 0.12 | 0.19 | 0.13 | 0.15 |
| 4 | 950 FLFb | 6.7 | 319/75/180 | 1.5 | 2.00 | 1.9 | 1.74 | 2.42 | 2.17 |
| 5 | 1170 BSF | 7.2 | 150/85/−170 | −0.2 | −0.65 | −0.60 | −0.5 | −0.75 | −0.70 |
| 6 | 1375 IVF | 7.1 | 18/60/−90 | 0.30 | 0.88 | 1.12 | 1.61 | 1.05 | 1.08 |
| 7 | 1453 GAF | 7.7 | 75/90/0 | 0.01 | 0.21 | 0.18 | 0.27 | 0.22 | 0.23 |
| 8 | 1557 PVF | 7.1 | 158/80/−175 | 3.06 | 4.95 | 7.11 | 11.45 | 10.25 | 9.50 |
| 9 | 1600 MRF | 7.0 | 2/60/−90 | 3.04 | 5.34 | 6.53 | 8.57 | 7.08 | 6.97 |
| 10 | 1605 GF | 7.2 | 1/60/−90 | 0.96 | 3.11 | 3.97 | 5.57 | 4.55 | 4.39 |
| 11 | 1715 FCF | 7.2 | 143/90/180 | 1.10 | 2.82 | 3.21 | 3.10 | 3.20 | 3.18 |
| 12 | 1872 OVF | 7.5 | 340/85/−172 | −0.07 | 0.71 | 0.68 | 0.63 | 0.99 | 1.06 |
| 13 | 1915 PSF | 7.5 | 198/50/−90 | 0.02 | 0.30 | 0.36 | 0.47 | 0.36 | 0.40 |
| 14 | 1932 CMF | 7.2 | 343/85/−175 | 0.18 | 0.56 | 1.25 | 2.35 | 1.11 | 1.25 |
| 15 | 1954 RMF | 7.0[d] | 8/55/−159 | 0.15 | 1.90 | 1.87 | 1.82 | 1.94 | 2.04 |
| 16 | 1954 FPF | 7.1 | 9/60/−140 | 0.13 | 0.82 | 0.80 | 0.77 | 1.22 | 1.10 |
| 17 | 1954 DVF | 7.2 | 37/35/−90 | 0.60 | 1.47 | 1.68 | 2.10 | 1.67 | 1.80 |

[a]Maximum calculated ΔCFS along the fault plane for the paleoseimological events; ΔCFS at hypocenter for the historical earthquakes.
[b]AVF, Antelope Valley Fault; PLF, Pyramid Lake Fault; FLFa, Fish Lake Valley Fault (Leidy Creek segment); FLFb, Fish Lake Valley Fault (Oasis segment); BSF, Benton Spring Fault; GAF, Garlock Fault; IVF, Incline Village Fault; PVF, Panamint Valley Fault; MRF, Mont Rose Fault; GF, Genoa Fault; FCF, Furnace Creek Fault; OVF, Owens Valley Fault; PSF, Pleasant Valley Fault; CMF, Cedar Mountain Fault; RMF, Rainbow Mountain Fault; FPF, Fairview Peak Fault; DVF, Dixie Valley Fault.
[c]Aki and Richards convention.
[d]Modeled as a single event.

(Figure 2), characterized by a complex pattern of right-lateral surface ruptures along a ~60 km long NNW-SSE striking zone [*Bell et al*., 1999]. Finally, between 6 July and 12 December 1954, five $M_w$ 6.4 to 7.2 events occurred in the Central Nevada Seismic Belt (CNSB). The first three events produced several right-lateral transtensional ruptures, forming a 70 km long fault zone that includes the Rainbow Mountain Fault (RMF) and other previously unmapped structures [*Bell et al*., 2004; *Caskey et al*., 2004]. Four months after the third event, the sequence moved to the east where a $M_w$ 7.2 earthquake ruptured the ~35 km long Fairview Peak Fault (FPF) and other smaller structures, producing right-lateral offsets up to 2.9 m and fault scarps up to 3.8 m high [*Caskey et al*., 1996]. This was followed within a few minutes by the $M_w$ 7.1 Dixie Valley earthquake (DVF), with maximum normal offsets of 2.8 m along a 42 km long fault rupture [*Caskey et al*., 1996]. The 1954 Dixie Valley earthquake (DVF) is the last major event in the region of interest to date.

### 2.2. Paleoseismological Earthquakes (587 A.D. to 1715 A.D.) and Their Source Faults

We collected data from several studies in order to define the age and the faults responsible for paleoseismological events that occurred in our study region in the last 1400 years (a detailed description of the data and the relevant references can be found in the supporting information, Data Set S2). The exact date of occurrence of each modeled earthquake is needed for the postseismic ΔCFS calculations. An exact date is of course not available for paleoearthquakes, which are characterized by large uncertainties. In such cases we take the mean value in the age range for the event and then subtract this value from the A.D. 1950 baseline. For the most recent event on the Antelope Valley fault, for example, we calculated the average (1363 years) within the $2\sigma$ uncertainty in the radiocarbon age (1312 and 1414 years B.P.) for the most recent event identified by *Sarmiento et al*. [2011]. Then we subtracted this calculated value from the A.D. 1950 baseline, resulting in an absolute age of A.D. 587. In this way we can have a reasonable "year of occurrence" to use as input for stress calculations. Because most paleoearthquakes have a fairly large age uncertainty, we also had to verify how this might change our result. This is addressed in section 5.1. All modeled earthquakes with absolute year of occurrence, magnitude, and fault kinematics are listed in Table 1.

### 2.3. Fault Slip Rates

Slip rate values are needed in order to calculate the interseismic ΔCFS (tectonic loading). A single fault, however, may have been assigned multiple slip rates by different authors. In particular, values derived from

geodesy are often different from those derived from geology for the same fault. A justification for the selection of slip rates used in our models is therefore needed.

First of all, geologic and geodetic slip rates apply to different timescales: geologic rates are usually applicable to periods of $10^3$–$10^6$ years, whereas geodetic rates are short term (0–20 years). Geologic slip rates, in addition, may be strongly timescale-dependent. In the Basin and Range province this has been documented, for example, on the Wassuk Range fault [*Surpless and Kroeger*, 2015], for which variations in vertical displacement rate were documented across 6 temporal orders of magnitude, and on the Wasatch fault, where different rates are observed at $10^3$, $10^5$, and $10^6$ timescales [*Friedrich et al.*, 2003]. Given that our period of interest is 1400 years, we use Holocene or late Pleistocene geologic slip rates ($10^3$–$10^4$ years) to calculate the interseismic ΔCFS accumulated by the main active faults (all values used and their references are listed in the supporting information, Data Set S3).

## 3. Methods

### 3.1. Modeling Coulomb Failure Stress Changes

Earthquake interactions have been widely explored since the 1980s using the concept of Coulomb stress changes [e.g., *King et al.*, 1994; *Stein et al.*, 1994, 1997; *Harris and Simpson*, 1998; *Stein*, 1999; *Parsons et al.*, 2000; *Marsan*, 2003; *Ma et al.*, 2005; *Toda et al.*, 2008].

The change in Coulomb failure stress (ΔCFS) caused by an earthquake is

$$\Delta\mathrm{CFS} = \Delta\tau - \mu'(\Delta\sigma_\mathrm{n}) \quad (1)$$

where $\Delta\tau$ is the change in shear stress calculated on the orientation and kinematics of either optimally oriented faults or specified faults, $\mu'$ is the coefficient of effective friction, and $\Delta\sigma_\mathrm{n}$ is the change in normal stress. A receiver fault located in an area of positive ΔCFS will be brought closer to failure, whereas failure will be delayed on a fault located in an area of negative ΔCFS. Coulomb stress changes due to earthquakes can be static (coseismic), quasi-static (postseismic), or dynamic [*Freed*, 2005]. The latter represent a transient effect due to seismic wave propagation and are believed to trigger seismicity only over a time period of days to months [*Freed*, 2005]. Because here we operate on a time span of 1400 years, we consider only coseismic (time-independent) and postseismic (time-dependent) Coulomb stress changes.

Coseismic stress changes are most useful to correlate events relatively close in time (0 to 10 years). When two events are widely separated in time instead, the postseismic effects due to relaxation of stresses in the lower crust and upper mantle can play an important role in the time-dependent redistribution of Coulomb stress and therefore may become the dominant process at the timescale considered in this work (1400 years) [e.g., *Chéry et al.*, 2001; *Pollitz et al.*, 2003; *Lorenzo-Martín et al.*, 2006; *Ali et al.*, 2008; *Shan et al.*, 2013; *Verdecchia and Carena*, 2015]. The interseismic ΔCFS for all faults of interest also needs to be determined. This is especially important in our case, because at the timescale considered most of the faults show at least some tectonic loading, which in a few cases may be of a magnitude comparable to the postseismic ΔCFS.

The input parameters necessary for all ΔCFS calculations are the location, size (or better, slip distribution), kinematics, and 3-D geometry of the source fault, and 3-D geometry and kinematics of the receiver faults. These parameters have uncertainties that can be addressed either by applying reasonable assumptions (e.g., for fault geometry and slip distribution) or by exploring the entire parameter space (e.g., friction coefficient, rheology). We calculated coseismic and postseismic ΔCFS using the code PSGRN/PSCMP [*Wang et al.*, 2006], which is based on a multilayered viscoelastic half-space. This code is composed of two routines. The first one (PSGRN) calculates the time-dependent Green functions of a given layered viscoelastic half-space for different dislocation sources at different depths. The second one (PSCMP) uses PSGRN results to calculate coseismic and postseismic deformation by linear superposition [*Wang et al.*, 2006]. We calculated interseismic ΔCFS instead using the elastic half-space-based software Coulomb 3.3 [*Toda et al.*, 2011], applying the "back slip" or "virtual dislocation" method [*Savage*, 1983; *Deng and Sykes*, 1997; *Papadimitriou and Sykes*, 2001; *Verdecchia and Carena*, 2015].

### 3.2. Fault Geometry and Slip Models for Specific Earthquakes

Knowledge of geometry and slip models of source faults, and geometry and kinematics of receiver faults, is required for Coulomb stress modeling. These parameters can be obtained with a reasonable degree of detail

**Table 2.** Combinations of Crust and Mantle Viscosities ($\eta$) Tested

| | Thickness[a] (km) | Model 1 $\eta$ (Pa s) | Model 2[b] $\eta$ (Pa s) | Model 3[c] $\eta$ (Pa s) |
|---|---|---|---|---|
| Upper–middle crust | 16 | Elastic | Elastic | Elastic |
| Lower crust | 19 | $1 \times 10^{19}$ | $3.2 \times 10^{19}$ | $1 \times 10^{20}$ |
| Upper mantle | 65 | $1 \times 10^{19}$ | $3.2 \times 10^{18}$ | $3.2 \times 10^{18}$ |

[a] *Bassin et al.* [2000].
[b] *Hammond et al.* [2010].
[c] *Gourmelen and Amelung* [2005].

for recent, instrumentally recorded earthquakes. For paleoseismological earthquakes, we estimated the average slip for a given earthquake using empirical relationships among event magnitude, rupture length, width, area, and surface displacement [e.g., *Wells and Coppersmith*, 1994]. For some faults in particular (Antelope Valley, Benton Springs, Incline Village, Genoa, Panamint Valley, and Furnace Creek) we used the measured coseismic offsets (described for each fault in the supporting information, Data Set S2) to better define input parameters as slip distribution and magnitude of the event. For the Genoa Fault and the Garlock Fault paleoseismological data for a single event exist at multiple localities along the fault trace. This allowed us to better define both the extent of the coseismic rupture and the variation of coseismic slip along strike. For all other faults, we used a tapered slip distribution, with maximum values at the center of the fault tapering to zero at the tips along strike.

We modeled historical earthquakes by combining geological and seismological data. The surface rupture of the 1915 $M_w$ 7.5 Pleasant Valley earthquake has been mapped in detail by *Wallace* [1984]. We used this information together with the focal mechanism determined by *Doser* [1988] to constrain the geometry and slip model of this rupture. The source fault of the 1932 $M_w$ 7.2 Cedar Mountain earthquake has been modeled using the surface faulting data of *Bell et al.* [1999] and the focal mechanism determined by *Doser* [1988]. We have constructed the geometry and slip models of the faults responsible for the 1954 Rainbow Mountain-Fairview Peak sequence from the focal mechanisms of *Doser* [1986] and the coseismic rupture measurements of *Caskey et al.* [2004] (Rainbow Mountain) and *Caskey et al.* [1996] (Fairview Peak). In order to define the geometry of the 1954 earthquake segment of the Dixie Valley Fault, we used the seismic profiles of *Abbott et al.* [2001] in combination with geological data (surface faulting) from *Caskey et al.* [1996]. The source fault parameters for the 1872 $M_w$ 7.5 Owens Valley earthquake are from *Haddon et al.* [2016] and are based on surface rupture data alone. Due to the lack of constraints at depth, for all source faults we used a constant dip angle. $\Delta$CFS has always been calculated for the entire depth range considered (0–15 km), but here we are mainly interested in either the $\Delta$CFS value at the hypocenter location (for historical earthquakes) or the maximum $\Delta$CFS value along the fault (for paleoseismological earthquakes). We chose 10 km as an observation depth to be shown in all the figures, because the hypocenters of most of the moderate to large earthquakes in our study for which hypocentral depth is known are approximately at this depth. Fault geometry, kinematics, and slip models for source faults are provided as input file for PSGRN/PSCMP in the supporting information (Data Set S1).

### 3.3. Rheologic Models

The postseismic $\Delta$CFS, due to viscoelastic relaxation of lower crust and upper mantle, depends on the rheologic parameters used in the model. A Maxwell rheology [*Thatcher and Pollitz*, 2008], Burgers rheology [*Pollitz*, 2003], and power law rheology [*Freed and Bürgmann*, 2004] have all been proposed for the western United States. The differences in postseismic $\Delta$CFS among these models are, however, minor when calculated for time spans longer than 100 years [*Verdecchia and Carena*, 2015]. In this work we have therefore used a Maxwell rheology to calculate the postseismic $\Delta$CFS in the region. On the basis of the range of rheological parameters of the lithosphere proposed for the western United States [*Thatcher and Pollitz*, 2008, and references therein], and of our prior work in this region [*Verdecchia and Carena*, 2015], we tested three different models with a Maxwell rheology in our final calculations (Models 1, 2, and 3) (Table 2). Model 1 and Model 3 represent two end-members of relaxation time. In Model 1 most of the stress is quickly released in the first ~ 150 years, whereas for Model 3 relaxation times are much longer. Model 2 represents an average between the two end-members [*Verdecchia and Carena*, 2015]. In this model it becomes apparent that the viscosity value adopted for the lower crust (Table 2) strongly controls the rate at which stress is transferred back to the elastic crust. All the figures in this paper have been produced using Model 3. A brief explanation concerning the influence of choice of models on our results follows below.

**Table 3.** Minimum/Maximum Present-Day Cumulative ΔCFS ($\Delta CFS_{cum}$) for Different Rheologies and Effective Friction Coefficients ($\mu'$), Interseismic ΔCFS ($\Delta CFS_{int}$), and Minimum/Maximum Present-Day Total ΔCFS ($\Delta CFS_{tot}$) Calculated on Each Receiver Fault

| | | $\Delta CFS_{cum}$ (Bars) | | | $\Delta CFS_{cum}$ (Bars) | | | $\Delta CFS_{tot}$ (Bars) |
|---|---|---|---|---|---|---|---|---|
| | | Model 3 | | | Model 1 | Model 2 | $\Delta CFS_{int}$ (Bars) | Model 3 |
| Fault[a] | Strike/Dip/Rake[b] (deg) | $\mu'$ 0.2 | $\mu'$ 0.4 | $\mu'$ 0.8 | $\mu'$ 0.4 | $\mu'$ 0.4 | $\mu'$ 0.4 | $\mu'$ 0.4 |
| HMF (SV) | 336/85/−150 | −5.4/2.6 | −7.2/2.2 | −11.5/1.1 | −7.1/2.2 | −7.0/2.4 | 43.4[c] | 36.2/45.6 |
| HMF (HM) | 305/85/−150 | −2.3/4.1 | −2.2/4.2 | −2.5/4.7 | −2.3/4.1 | −2.2/4.1 | 37.8[c] | 35.6/42.0 |
| FLF | 320/80/180 | −1.7/8.5 | −1.3/9.5 | −0.5/8.6 | −2.3/9.8 | −1.9/9.1 | 35.0[d] | 33.7/44.5 |
| BMF | 165/60/−135 | 0.6/4.3 | 1.2/5.4 | 2.0/7.6 | 0.8/5.4 | 1.1/5.6 | 40.6[c] | 41.8/46.0 |
| WRF | 340/55/−90 | −4.6/3.2 | −5.7/3.9 | −8.0/5.5 | −6.3/4.4 | −6.1/4.2 | 14.7[c] | 9.0/18.6 |
| HLF | 310/90/180 | 0.4/0.6 | 0.3/0.6 | 0.3/0.5 | 0.2/0.5 | 0.3/0.6 | 26.6[c] | 26.9/27.2 |
| PLF | 340/85/180 | 0.6/1.8 | 0.5/1.6 | 0.3/1.5 | 0.2/1.6 | 0.4/1.9 | 35.1[e] | 34.6/36.7 |
| MFS | 332/90/180 | 0.0/0.3 | 0.0/0.4 | 0.0/0.6 | 0.0/0.5 | 0.0/0.6 | 21.0[c] | 21.0/21.4 |
| DVF (NS) | 37/35/−90 | −11.0/8.6 | −11.0/9.7 | −13.0/11.4 | −10.0/11.3 | −11.0/10.6 | 6.3[c] | −4.7/16.0 |
| WMF | 166/60/−140 | −22.3/8.8 | −24.0/9.6 | −25.7/8.7 | −21.8/10.7 | −22.1/10.6 | 19.6[c] | −4.4/29.2 |

[a]HMF (SV), Hunter Mountain (Saline Valley section); HMF (HM), Hunter Mountain (Hunter Mountain section); FLF, Fish Lake Valley; BMF, Black Mountain; WRF, Wassuk Range; HLF, Honey Lake, PLF, Pyramid Lake; MFS, Mohawk; DVF (NS), Dixie Valley (northern segment); WMF, White Mountain.
[b]Aki and Richards convention.
[c]Calculated over 1400 years.
[d]Calculated over 1000 years.
[e]Calculated over 1300 years.

### 3.4. Influence of Effective Fault Friction and of Viscosity of the Lower Crust and Upper Mantle on the Results

The coefficient of effective friction ($\mu'$) and the viscosity ($\eta$) of the lower crust and upper mantle play an important role in ΔCFS calculations. Effective friction, as it can be seen in equation (1), controls the value of the normal stress component. Viscosity instead influences the rate at which stresses are transferred to the upper crust. Both of these parameters may thus affect the stability of our results, and therefore they need to be considered.

In order to test the effect of varying $\mu'$ and $\eta$, we followed the same approach as *Verdecchia and Carena* [2015]. In addition to the three different rheological models discussed in section 3.3, we calculated $\Delta CFS_{cum}$ for three different values of $\mu'$ (0.2, 0.4, and 0.8) (Tables 1 and 3). In the supporting information (Figures S5–S7) graphical examples of $\Delta CFS_{cum}$ calculated with $\mu'$ of 0.2 and 0.8 are shown as well.

The results of these tests indicate that both $\mu'$ and $\eta$ control mainly the magnitude of $\Delta CFS_{cum}$, as also observed by *Verdecchia and Carena* [2015] on a 150 year timescale. Slightly different magnitudes of stress loading and stress shadows are observed for different values of $\mu'$, but this does not affect the sign of the Coulomb stress changes on the receiver faults. Based on the considerations above, we have drawn our general conclusions from simulations carried out using a value of effective friction of 0.4 and the rheology of Model 3, which represents the most conservative of all the rheological models considered.

## 4. Results

Starting with the 587 $M_w$ 7.2 Antelope Valley earthquake and ending with the 1954 $M_w$ 7.2 Dixie Valley earthquake, we determined both the $\Delta CFS_{cum}$ for each of the 17 studied faults immediately before the occurrence of each earthquake and the present-day $\Delta CFS_{tot}$ on the major faults in the region. In order to make it easier to follow the description of our results below, we have divided the region into three subregions: (1) northern ECSZ, (2) central Walker Lane-western Basin and Range, and (3) northwestern Walker Lane. This subdivision takes into account the fact that in terms of the stress transfer patterns obtained in this work, faults within the same subregion strongly interact, whereas from one region to the next such interactions are less significant.

### 4.1. Cumulative ΔCFS in the Northern ECSZ

The two surface-rupturing events on the Fish Lake Valley Fault (913 $M_w$ 6.8 Leidy Creek segment and 950 $M_w$ 6.7 Oasis segment) are the oldest earthquakes in our model that occurred in the northern ECSZ. The first event transferred ~2 bars of positive $\Delta CFS_{cum}$ to the segment responsible for the second event (Table 1

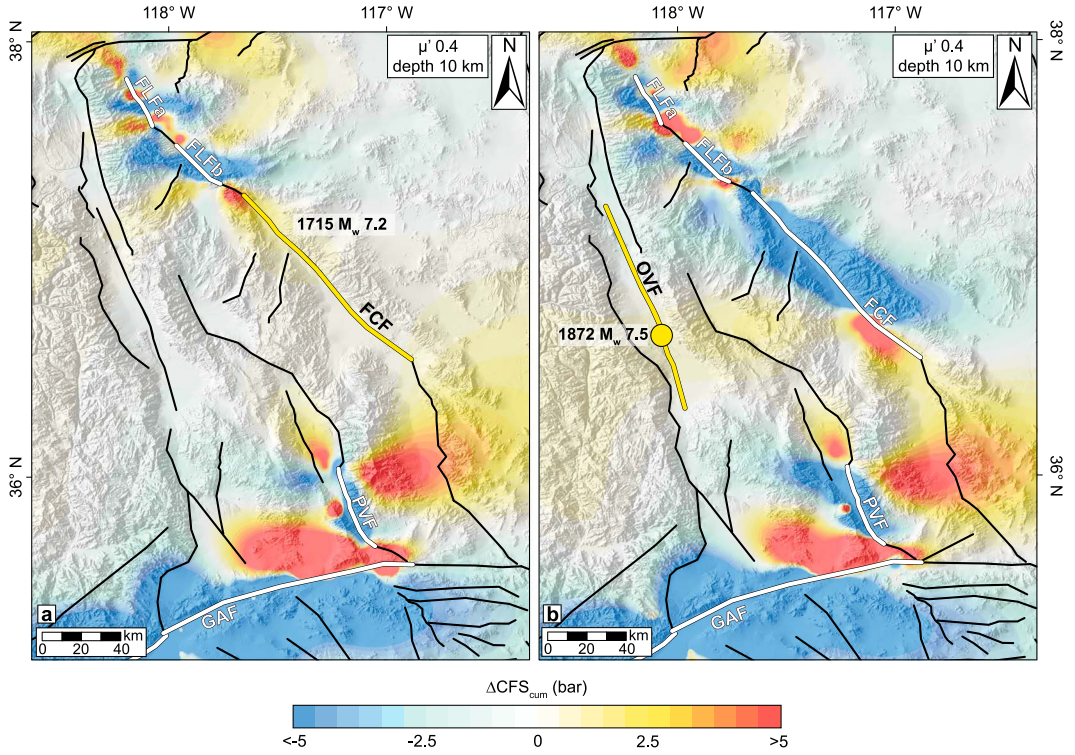


**Figure 3.** Cumulative ΔCFS due to all previous events resolved (a) on the kinematics of the Furnace Creek Fault (FCF) just before the 1715 earthquake and (b) on the kinematics of the Owens Valley Fault (OVF) just before the 1872 earthquake (yellow circle = earthquake epicenter). Thick white lines are source faults; thick yellow lines are receiver faults. FLFa, Fish Lake Valley Fault (Leidy Creek segment); FLFb, Fish Lake Valley Fault (Oasis segment); GAF, Garlock Fault; PVF, Panamint Valley Fault.

and Figure S2c), and together these two earthquakes increased stresses further on the Furnace Creek Fault, responsible for the 1715 $M_w$ 7.2 earthquake (Figure 3a). The Furnace Creek event in turn produced a positive $\Delta CFS_{cum}$ in Owens Valley (Figure 3b), at the location where an $M_w$ 7.5 earthquake occurred in 1872.

The $\Delta CFS_{cum}$ on the Garlock Fault just prior to the 1453 $M_w$ 7.7 event is small (0.2 bar) but still positive (Table 1 and Figure S3b). The $\Delta CFS_{cum}$ of the 1453 earthquake largely contributed to the occurrence of the 1557 $M_w$ 7.1 Panamint Valley earthquake, by producing a positive stress increase all along the fault with a maximum value of ~7 bars (Table 1 and Figure S3c).

### 4.2. Cumulative ΔCFS in the Central Walker Lane-Western Basin and Range

In the central Walker Lane the 1170 $M_w$ 7.2 Benton Springs earthquake increased $\Delta CFS_{cum}$ on the northernmost part of the Cedar Mountain Fault, whereas negative $\Delta CFS_{cum}$ accumulated in the central and southern part of the same fault. The 1932 $M_w$ 7.2 earthquake occurred [*Doser*, 1988] in the area of positive $\Delta CFS_{cum}$ (Figure 4a). Together with the 700 $M_w$ 7.0 Pyramid Lake earthquake, the 1915 $M_w$ 7.5 Pleasant Valley earthquake, and the 1932 $M_w$ 7.2 Cedar Mountain earthquake, the 1170 Benton Springs earthquake also produced a large area of positive $\Delta CFS_{cum}$ in the region where the 1954 Rainbow Mountain-Fairview Peak-Dixie Valley earthquake sequence later occurred (Figure 4b). The 700 $M_w$ 7.0 Pyramid Lake event also slightly increased $\Delta CFS_{cum}$ (~0.4 bar) at the location of the 1915 $M_w$ 7.5 Pleasant Valley earthquake (Table 1 and Figure S4a).

### 4.3. Cumulative ΔCFS in the Northwestern Walker Lane

The 587 $M_w$ 7.2 Antelope Valley and the 700 $M_w$ 7.0 Pyramid Lake earthquakes are the oldest events modeled in this study. The Antelope Valley earthquake first produced a small $\Delta CFS_{cum}$ increase (0.2–0.3 bar) on the Pyramid Lake Fault (Table 1 and Figure S2a). Then the two events combined transferred significant positive $\Delta CFS_{cum}$ to the Carson Range and Lake Tahoe region (Figure 5a), where in 1375 the Incline Village Fault and

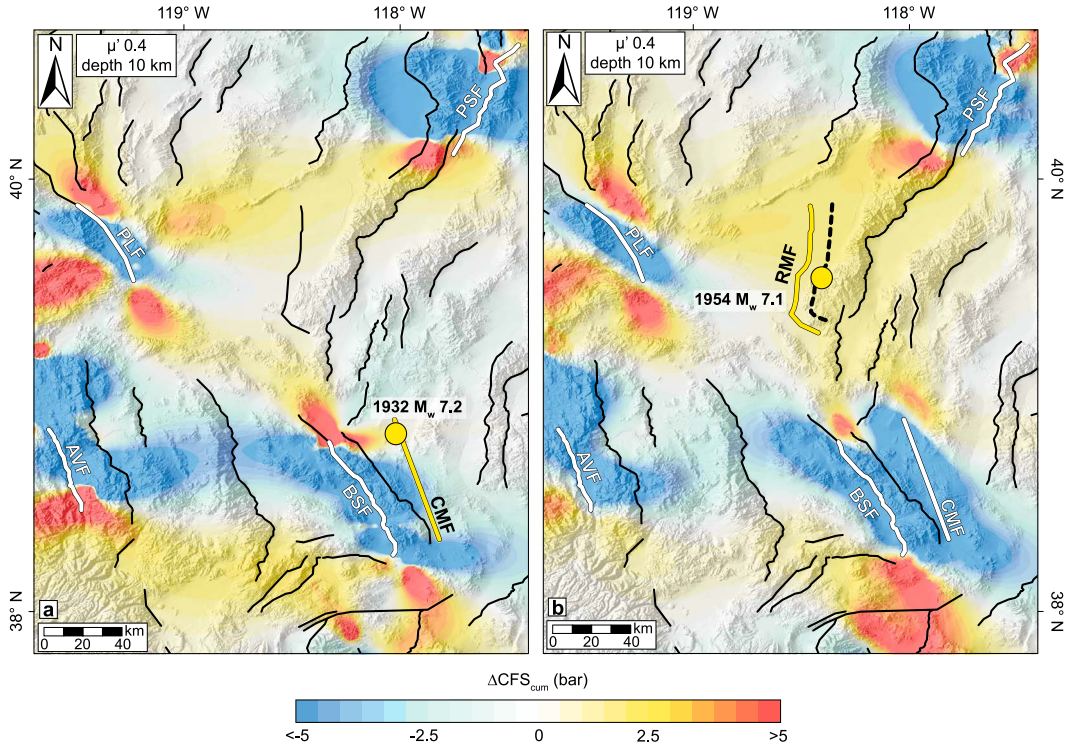


**Figure 4.** Cumulative ΔCFS due to all previous events resolved (a) on the kinematics of the Cedar Mountain Fault (CMF) just before the 1932 earthquake and (b) on the kinematics of the Rainbow Mountain Fault (RMF) just before the 1954 earthquake. Thick white lines are the source faults; thick yellow lines are receiver faults, dashed black lines represent the depth contour of the receiver fault at calculation depth; yellow circles are earthquake epicenters. AVF, Antelope Valley Fault; BSF, Benton Springs Fault; PLF, Pyramid Lake Fault; PSF, Pleasant Valley Fault.

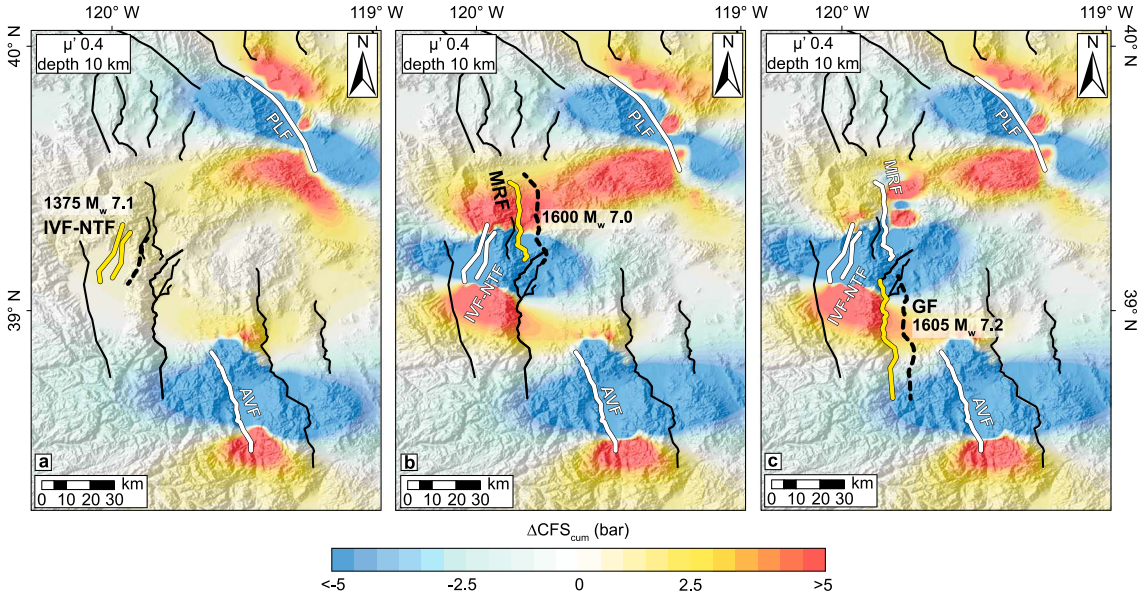


**Figure 5.** Cumulative ΔCFS due to all previous events resolved (a) on the kinematics of the Incline Village-North Tahoe Fault (IVF-NTF) just before the 1375 earthquake, (b) on the kinematics of the Mount Rose Fault (MRF) just before the 1600 earthquake, and (c) on the kinematics of the Genoa Fault (GF) just before the 1605 earthquake. Thick white lines are source faults; thick yellow lines are receiver faults; dashed black lines represent the depth contour of the receiver fault at calculation depth. AVF, Antelope Valley Fault; PLF, Pyramid Lake Fault.

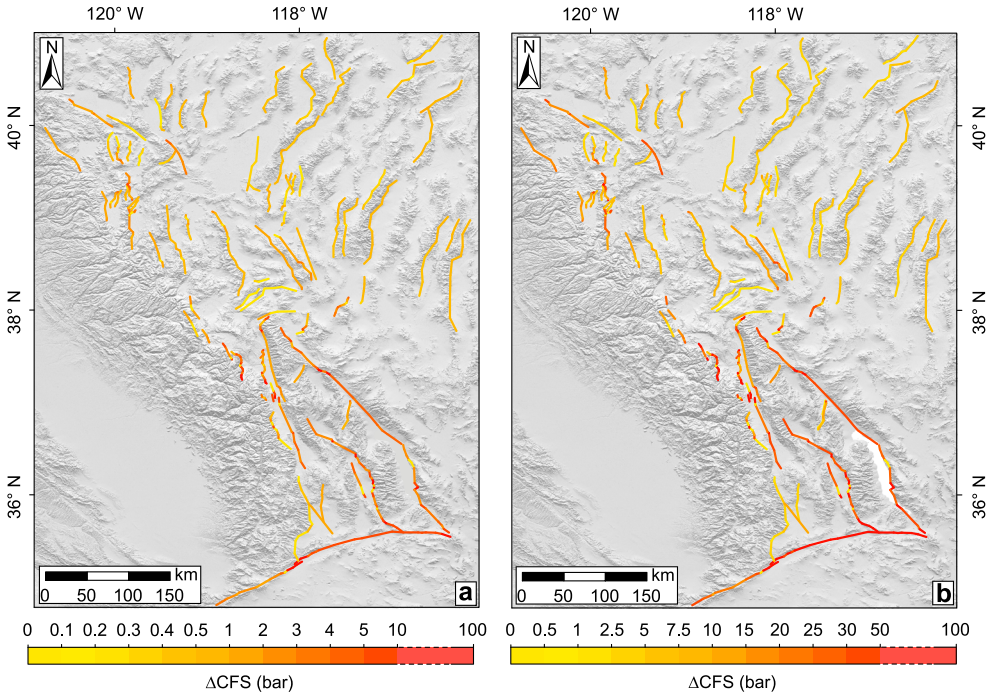


**Figure 6.** Interseismic ΔCFS (tectonic loading) for a time interval of (a) 100 years and (b) 1000 years, calculated with the back slip method [*Savage*, 1983] on the orientation and kinematics of each modeled fault. For each segment, the maximum interseismic ΔCFS is shown, regardless of depth.

the North Tahoe Fault ruptured together producing an $M_w$ 7.1 earthquake. This earthquake then increased the stress on the central segment of the Genoa fault and on the northern part of the Mount Rose Fault, whereas it produced a stress drop on the northern segment of the Genoa Fault and on the southern segment of the Mount Rose Fault (Figure 5b). These faults ruptured ~250 years later, possibly in two events very close to each other in time [*Ramelli and Bell*, 2009], with the first earthquake transferring positive $\Delta CFS_{cum}$ (~4 bars) on the fault segment responsible for the next event.

### 4.4. Present-Day Total ΔCFS in the Northern ECSZ, Walker Lane, and Western Basin and Range

In this region there are also several prominent faults that did not produce any major surface-rupturing event in the 1400 years considered in our study. Some examples are the Black Mountain [*Klinger and Piety*, 2001; *Sohn et al*., 2014], Hunter Mountain [*Oswald and Wesnousky*, 2002], and White Mountain faults [*Kirby et al*., 2006] in the northern ECSZ; the Wassuk Range [*Wesnousky*, 2005; *Bormann et al*., 2012], Honey Lake [*Turner et al*., 2008], and Mohawk faults [*Gold et al*., 2014] in the Walker Lane; and the northern segment of the Dixie Valley fault [*Bell et al*., 2004] in the western Basin and Range. Here we calculated the $\Delta CFS_{tot}$ accumulated by each of these faults in the last 1400 years by adding the interseismic ΔCFS (Figure 6 and Table 3) to the $\Delta CFS_{cum}$ produced by all the studied events combined. We also calculated the $\Delta CFS_{tot}$ on the Pyramid Lake Fault and Fish Lake Fault for the last 1300 and 1000 years, respectively (Table 3), because the age of the most recent event for these faults is comparable with their average recurrence interval [*Sawyer and Reheis*, 1999; *Briggs and Wesnousky*, 2004], and therefore they may be close to failure. According to our results, only four of the studied faults (Black Mountain, Honey Lake, Mohawk, and Pyramid Lake faults) have accumulated positive $\Delta CFS_{cum}$ along their entire length, whereas the rest are characterized by a heterogeneous $\Delta CFS_{cum}$ distribution. Figure 7a shows 1400 years of $\Delta CFS_{cum}$ for the Black Mountain Fault. This fault has accumulated a maximum of ~6 bars of $\Delta CFS_{cum}$ (Table 3), mostly due to the effect of the 1557 $M_w$ 7.1 Panamint Valley earthquake. Adding to this the large interseismic ΔCFS, the $\Delta CFS_{tot}$ in the southern part of the fault is ~46 bars (Table 3).

The Honey Lake and the Mohawk faults have accumulated a maximum of 0.6 and 0.4 bar of positive $\Delta CFS_{cum}$, respectively (Table 3 and Figures 7b and 7c), which represent a very small part of the ~30 bars of $\Delta CFS_{tot}$ calculated on the Honey Lake Fault and ~21 bars calculated on the Mohawk Fault. The interseismic loading

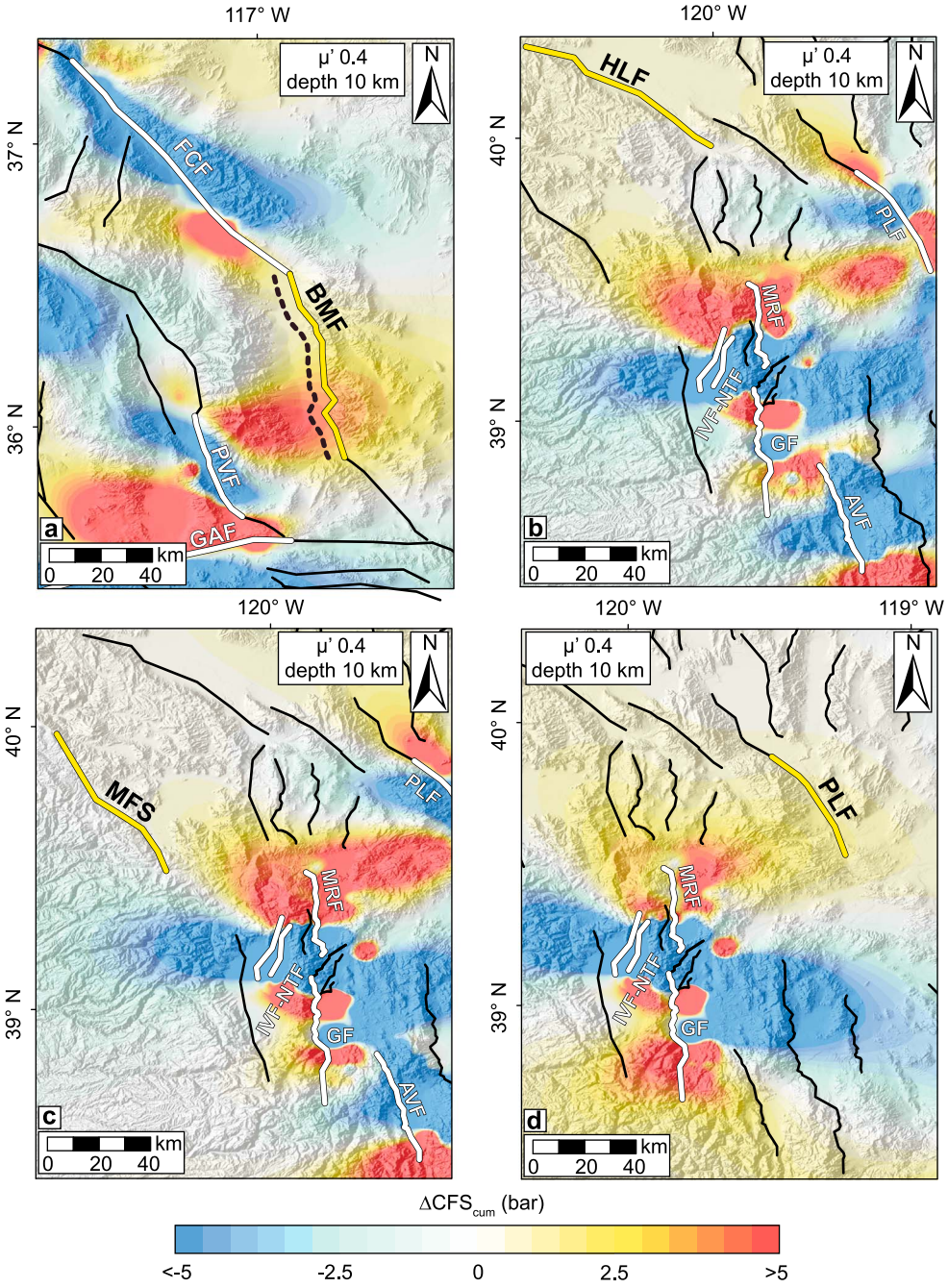


**Figure 7.** Cumulative ΔCFS from all the studied event combined, calculated (a) on the kinematics of the Black Mountains Fault (BMF), (b) on the kinematics of the Honey Lake Fault (HLF), (c) on the kinematics of the Mohawk fault system (MFS) and (d) on the kinematics of the Pyramid Lake Fault (PLF). Thick white lines are the source faults; thick yellow lines are receiver faults; dashed black lines represent the depth contour of the receiver fault at calculation depth. AVF, Antelope Valley Fault; GF, Genoa Fault; GAF, Garlock Fault; IVF-NTF, Incline Village-North Tahoe Fault; MRF, Mount Rose Fault; PVF, Panamint Valley Fault.

forms also a large contribution to the $\Delta CFS_{tot}$ accumulated by the Pyramid Lake Fault (~37 bars, of which only ~ 1.5 bars are due to $\Delta CFS_{cum}$) (Table 3 and Figure 7d).

The Hunter Mountain Fault has been consistently unloaded along most of its length. Positive $\Delta CFS_{cum}$ were calculated only in a small region between the southern Saline Valley section and the northern Hunter Mountain section with maximum values of about 4.2 bars. Both the Hunter Mountain section and the

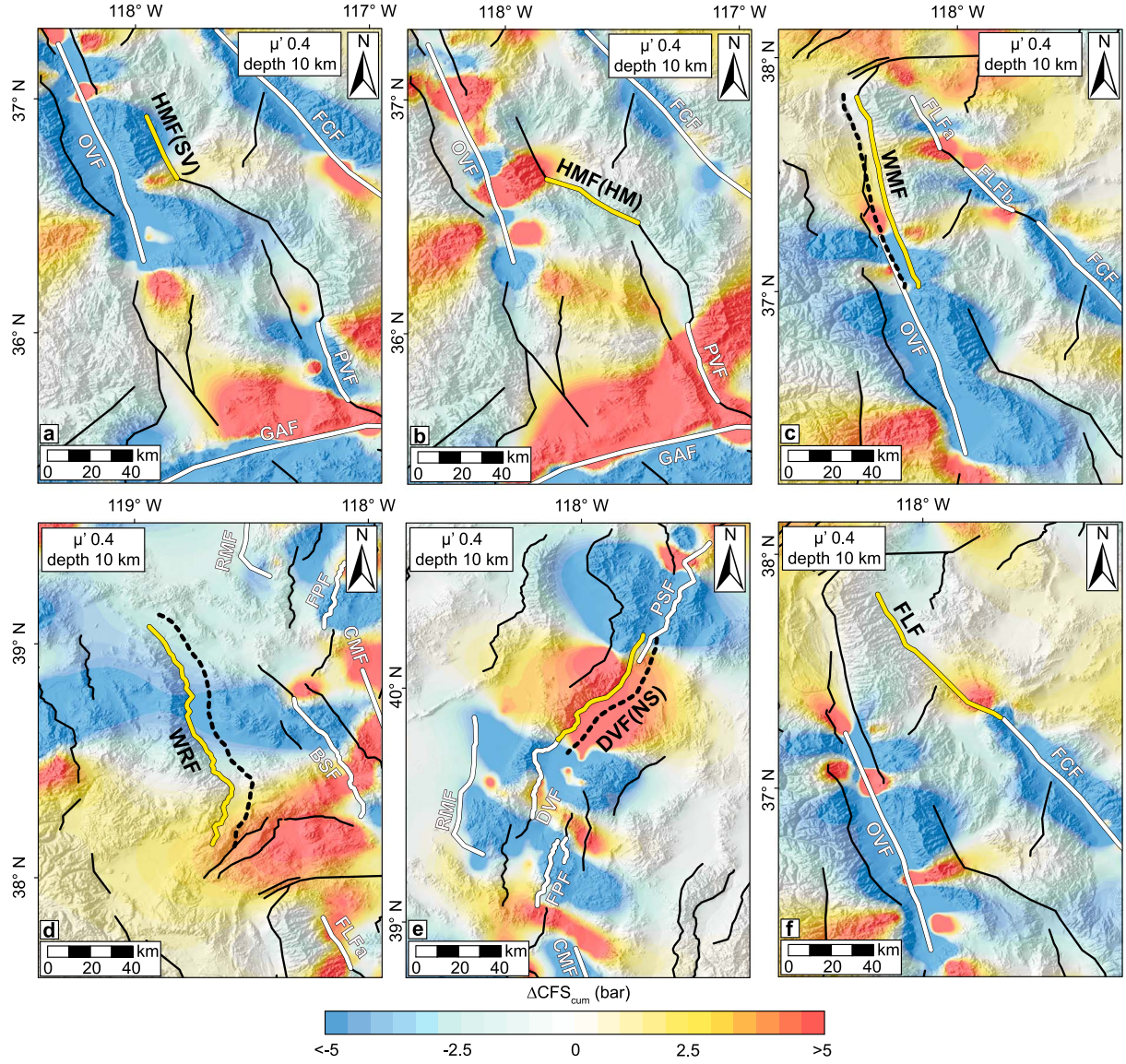


**Figure 8.** Cumulative ΔCFS from all the studied event combined, calculated (a) on the kinematics of the Saline Valley section of the Hunter Mountain Fault (HMF(SV)), (b) on the kinematics of the Hunter Mountain section of the Hunter Mountain Fault (HMF(HM)), (c) on the kinematics of the White Mountains Fault (WMF), (d) on the kinematics of the Wassuk Range Fault (WRF), (e) on the kinematics of the Dixie Valley Fault (northern segment) (DVF(NS)), and (f) on the kinematics of the Fish Lake Valley Fault (FLF). Thick white lines are the source faults; thick yellow lines are receiver faults; dashed black lines represent the depth contour of the receiver fault at calculation depth. BSF, Benton Springs Fault; CMF, Cedar Mountain Fault; DVF, Dixie Valley Fault; FCF, Furnace Creek fault; FLFa, Fish Lake Valley Fault (Leidy Creek segment); FLFb, Fish Lake Valley Fault (Oasis segment); FPF, Fairview Peak Fault; GAF, Garlock fault; OVF, Owens Valley fault; PSF, Pleasant Valley Fault; PVF, Panamint Valley fault; RMF, Rainbow Mountain Fault.

Saline Valley section instead experienced a negative $\Delta CFS_{cum}$ of −2.2 bars and −7.2 bars, respectively (Table 3 and Figures 8a and 8b). However, the high interseismic ΔCFS entirely erased the stress shadow and loaded the Hunter Mountain Fault. The maximum $\Delta CFS_{tot}$ on this fault is ~36 bars in the region characterized by negative $\Delta CFS_{cum}$ and ~45 bars in the region with positive $\Delta CFS_{cum}$ (Table 3).

The White Mountain Fault experienced ~10 bars of maximum positive $\Delta CFS_{cum}$ in its central segment (Table 3 and Figure 8c) due to the 1872 $M_w$ 7.5 Owens Valley earthquake. The addition of interseismic stress results in a $\Delta CFS_{tot}$ of ~ 30 bars. The southernmost part of the fault is instead located in a region of large stress drop due to the fact that it is parallel to the Owens Valley Fault, and as a result also the $\Delta CFS_{tot}$ in this segment of the fault is negative (Table 3).

The Wassuk Range Fault is equally characterized by an inhomogeneous distribution of $\Delta CFS_{cum}$ (Table 3 and Figure 8d). While the northern part accumulated negative values of stress (~ −6 bars), the southern segment experienced a maximum $\Delta CFS_{cum}$ of ~ 4 bars. Adding the interseismic ΔCFS, the maximum $\Delta CFS_{tot}$ in the southern part of the fault is ~19 bars, and the minimum $\Delta CFS_{tot}$ in the northern part is ~ 9 bars.

The northern segment of the Dixie Valley Fault, located between the surface ruptures of the 1915 $M_w$ 7.5 Pleasant Valley earthquake to the north and the 1954 $M_w$ 7.2 Dixie Valley earthquake to the south, has accumulated a maximum positive $\Delta CFS_{cum}$ of ~10 bars (Table 3 and Figure 8e). Due to its low slip rate, the contribution of the interseismic stress is only ~ 6 bars in the last 1400 years, which results in a $\Delta CFS_{tot}$ of ~16 bars (Table 3).

Finally, Figure 8f shows the $\Delta CFS_{cum}$ for the Fish Lake Valley Fault. The southern part of this fault has been loaded by the 1715 $M_w$ 7.2 Furnace Creek earthquake, whereas a negative $\Delta CFS_{cum}$ (~ –1 bar) characterizes the northern part. Tectonic loading plays a major role in the $\Delta CFS_{tot}$ of the Fish Lake Valley Fault, which ranges between ~34 and ~45 bars.

## 5. Discussion

### 5.1. Significance of Observed Stress Patterns

Our most significant result is that 15 out of 16 modeled receiver faults are either partially or entirely located in regions of positive $\Delta CFS_{cum}$ due to all previous events (Table 1). This finding indicates that changes in stress distribution due to major earthquakes may control the location of subsequent events over a 1400 year timescale.

The magnitude of positive $\Delta CFS_{cum}$ that we calculated varies from 0.2 to 10 bars. Such values are relatively small compared to average earthquake stress drops, suggesting that most faults are likely close to failure most of the time and as a consequence even small stress perturbations (<1 bar) may affect the location of future events on suitably oriented faults. This has been already observed in the same region by *Verdecchia and Carena* [2015] and in other tectonically active regions worldwide by several other authors [*Stein et al*., 1997; *Pollitz et al*., 2003; *Freed et al*., 2007; *Scholz*, 2010].

Not all of the faults in our study area have been the focus of paleoseismological studies that aimed at identifying the most recent event on each. As a consequence, it is possible that some large unidentified event would modify the $\Delta CFS_{cum}$ evolution that we calculated. This is an uncertainty that can only be addressed when relevant additional data become available in the future. Even if the most recent event on a fault is known, it is often characterized by large age uncertainties. Therefore, the temporal order of our events sequence may change depending on which age we choose within the uncertainty range of each event. In our study this applies to the oldest events (587 Antelope Valley, 700 Pyramid Lake, 913 Leidy Creek segment, and 950 Oasis segment earthquakes). However, as described in section 4, the first two events belong to the northwestern Walker Lane and the other two to the northern ECSZ, and therefore the two pairs are too far and do not affect each other in terms of $\Delta CFS_{cum}$. Changing the relative position of the events inside each pair will not alter our results; the Pyramid Lake earthquake will produce a small positive (~0.2 bar) $\Delta CFS_{cum}$ on the Antelope Valley fault, whereas in the original sequence it is the 587 Antelope Valley earthquake that increases the stress on the Pyramid Lake Fault. The Oasis segment earthquake will strongly encourage faulting on the Leidy Creek segment of the Fish Lake Fault, while the opposite is happening in the modeled sequence. In both cases the combining effect of the earthquakes on the two segments will eventually increase stress on the Furnace Creek Fault, responsible for the subsequent 1715 event. A similar consideration also applies to the pair formed by the 1453 Garlock and 1557 Panamint Valley earthquakes, but, as also discussed by *McAuliffe et al*. [2013], these faults increase ΔCFS on each other, regardless of which of the two events struck first. Another case is that of the 1600 Mont Rose and the 1605 Genoa earthquakes. According to *Ramelli and Bell* [2009], these two earthquakes may have been very close in time, but the resolution of the data is not high enough to say which happened first. The order of these two earthquakes however does not affect our results, because one fault is the along-strike extension of the other, and therefore one fault loads the other regardless in which order the earthquakes occur.

An additional consideration concerning paleoseismological records is that in only a few cases (e.g., Genoa Fault and Garlock Fault) multiple paleoseismological sites along a fault are available where a specific earthquake was recorded. This produces uncertainties in the extent of the coseismic rupture, which we mainly

address by applying empirical relationships among event coseismic displacement, and magnitude [*Wells and Coppersmith*, 1994].

The presence outside of the study area of faults large enough to produce major earthquakes could change the state of stress on faults within the study area, affecting our results. An obvious example is the San Andreas Fault. *Freed et al*. [2007] found that the 1857 $M_w$ 8.2 Fort Tejon earthquake likely transferred positive $\Delta CFS_{cum}$ to the Owens Valley region and therefore contributed to the occurrence the 1872 Owens Valley earthquake. *McAuliffe et al*. [2013] suggested the possible interaction in terms of ΔCFS between the most recent event on the Garlock Fault [*Dawson et al*., 2003; *Madugo et al*., 2012] and the most recent event on the Mojave section of the San Andreas Fault [*Scharer et al*., 2011]. Including these events from the San Andreas Fault will not change the significance of our results. In the first case, in fact, the effect of the 1857 Fort Tejon earthquake would further increase the ΔCFS on the Owens Valley Fault, already brought toward failure by the 1717 Furnace Creek earthquake. In the second case, a possible event on the Mojave section of the San Andreas Fault would transfer positive ΔCFS to the Garlock Fault increasing the $\Delta CFS_{cum}$ accumulated by this fault to values larger than 2.5 bars [*McAuliffe et al*., 2013].

Several major faults in our study region do not seem to have produced any ground-rupturing events in the last 1400 years. If this is indeed real, as opposed to being the result of lack of sufficient information about the rupture history of these faults, it means that they have accumulated high values of $\Delta CFS_{tot}$, comparable with the average stress drop expected for moderate to major earthquakes (10 to 100 bars [*Hanks*, 1977; *Scholz*, 2002]). As a consequence, if we think in terms of time-dependent probability, these faults represent the most likely candidates for future major earthquakes in the region. Four large faults that appear not to have ruptured within the time range covered by this study are the Hunter Mountain Fault [*Oswald and Wesnousky*, 2002], the Black Mountain Fault [*Klinger and Piety*, 2001; *Sohn et al*., 2014; *Frankel et al*., 2016], the Honey Lake Fault [*Turner et al*., 2008], and the White Mountains Fault [*Kirby et al*., 2006] (Table 3 and Figures 7 and 8). Because the most recent events on the Fish Lake Fault [*Reheis*, 1994*; Reheis et al*., 1995] and Pyramid Lake Fault [*Briggs and Wesnousky*, 2004] occurred, respectively, ~1000 years and ~1300 years B.P., these two faults have also had enough time to accumulate significant values (10 to 100 bars) of $\Delta CFS_{tot}$. Unfortunately, for some of these faults there are limited paleoseismological data. The age of the most recent event on the White Mountains Fault and the Hunter Mountain Fault, for instance, is unknown. Scarp morphology analysis results from different sections of the Black Mountain Fault show different ages for the most recent event in each section. *Machette et al*. [1999] estimated an age of 500–840 years for the most recent faulting event on the northern section. *Klinger and Piety* [2001] found evidences for a Mid-Holocene event on the central section and for a 1000–2000 year old event on the southern section. *Frankel et al*. [2016] used optically stimulated luminescence dating to define a maximum age of ~ 4.5 ka for the most recent event on the central part of the Black Mountain Fault (Badwater site). The authors concluded that the 6.4 m tall scarp measured at the studied location could be the result of at least two surface-rupturing events. The Pyramid Lake, Fish Lake, and Honey Lake faults are the only faults in this group for which trench studies have been completed. The available data and the relative uncertainties for the first two are described in detail in the supporting information, Data Set S2. The Honey Lake Fault has been studied by *Turner et al*. [2008], who reported one surface-rupturing earthquake post ~4670 years B.P. Because of the limited stratigraphy at the study site, the authors, however, did not rule out the possibility of additional younger events.

Even considering the lack of detailed paleoseismological studies (especially for the White Mountains, Hunter Mountain, and Black Mountain faults), and the uncertainties in the age of the most recent event for all faults, we believe that these six faults are the most likely candidates for the next major earthquake in the region. The White Mountains Fault is the only one of these faults that falls into areas of both positive and negative $\Delta CFS_{tot}$ (Table 3). We speculate that because its southern segment is still located in a region of negative $\Delta CFS_{tot}$, a future rupture may be limited to the central and northern parts of this fault.

Discrepancies between geologic and geodetic slip rates have been widely observed in the Walker Lane and in the northern Eastern California Shear Zone [*Oskin et al*., 2008; *Frankel et al*., 2011; *Amos et al*., 2013]. *Peltzer et al*. [2001], using InSAR data for the region where the Garlock Fault and the Eastern California Shear Zone intersect, observed deformation rates inconsistent with geological data, particularly in the region around the Little Lake Fault. The authors proposed that this ongoing rapid deformation could be the result of postseismic processes from the 1872 Owens Valley earthquake and the 1992 Landers earthquake. Although the 1992 Landers

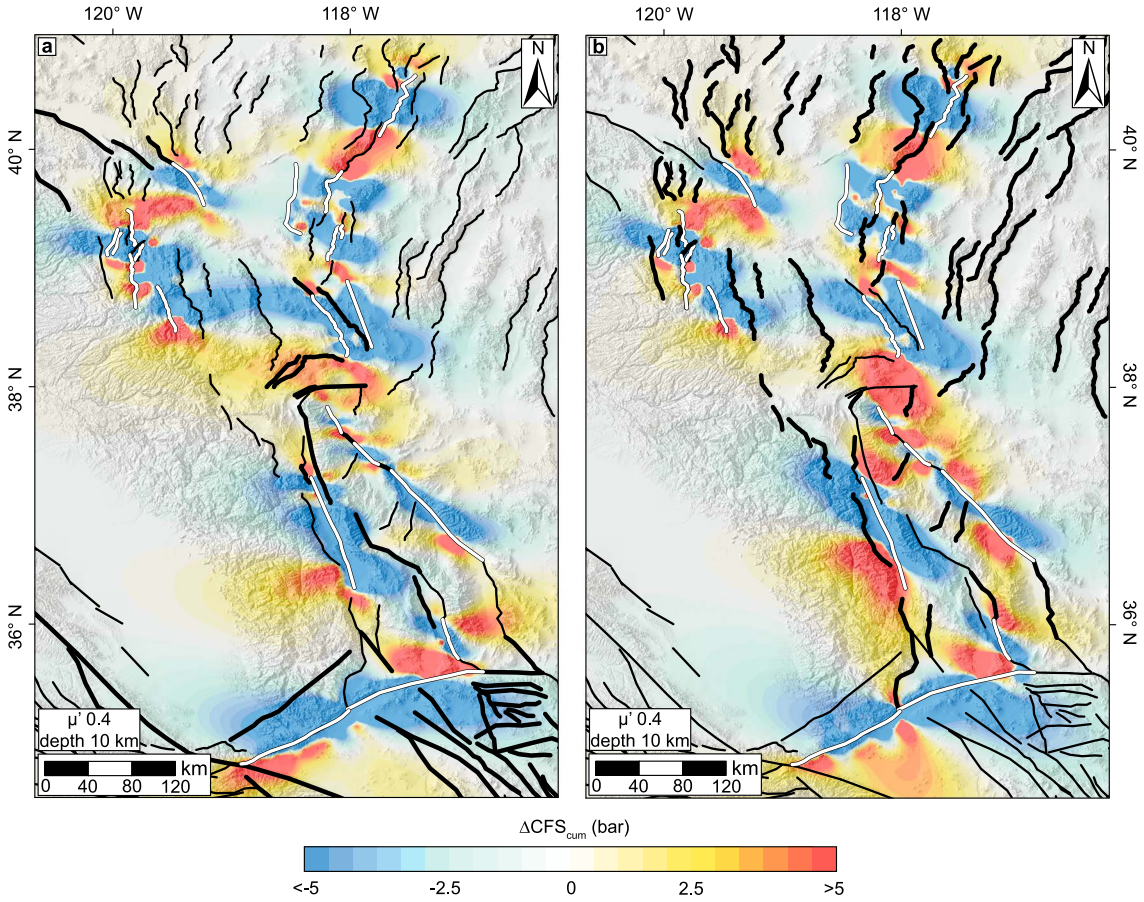


**Figure 9.** Present-day cumulative ΔCFS from all the studied events combined, calculated (a) on optimally oriented strike-slip faults, and (b) on optimally oriented normal faults. Thick white lines are the source faults. Thick black lines are faults with dominantly strike-slip kinematics in Figure 9a, and dominantly normal kinematics in Figure 9b.

earthquake is not part of our study, our results (Figures 9a and 9b) show that the Little Lake Fault is located in a region of positive $\Delta CFS_{cum}$ produced by the 1872 Owens Valley earthquake and by the 1605 Garlock Fault earthquake. Concentrated postseismic ΔCFS produced by several source faults may therefore control the location of temporary rapid deformation and clustering of events, as it is presently happening around the Little Lake Fault. The cluster of events that occurred in 1954 in the Rainbow Mountain-Fairview Peak-Dixie Valley region may have been an analogue case in the past. In this region several previous earthquakes had created a large area of positive $\Delta CFS_{cum}$ facilitating the occurrence of the 1954 sequence (Figure 4b).

### 5.2. Statistical Significance of Our Results

In order to verify whether the results that most source faults are in areas of positive $\Delta CFS_{cum}$ can be obtained by chance, we performed 10 tests on random earthquake sequences. From our study region, we chose 67 active faults large enough to produce ground-rupturing earthquakes (these include also all those faults for which there is no record of any earthquakes in the last 1400 years). We then created 10 sequences of 17 random source faults (i.e., earthquakes) with the same date of occurrence and event magnitude as those of our real sequence and performed $\Delta CFS_{cum}$ calculations for each of the 10 sequences. The results are shown in Table 4.

In the actual sequence, ~80% of the source faults are partially or fully located in areas of $\Delta CFS_{cum} \geq 0.2$, and ~70% are in areas of $\Delta CFS_{cum} \geq 0.4$. In none of the random tests could these percentages be reproduced. In fact, as expected for a random process, on average the events fell in areas of increased $\Delta CFS_{cum}$ only about 50% of the time.

**Table 4.** Comparison of Cumulative ΔCFS Between the Actual Earthquake Sequence and Ten Control Tests on Random Faults and Earthquakes

| Earthquake Sequence | ΔCFS ≥ 0.2 Bar | ΔCFS ≥ 0.4 Bar | Full ΔCFS > 0[a] |
|---|---|---|---|
| Actual sequence | 13 (81%) | 11 (69%) | 9 (56%) |
| Test 1 | 9 (56%) | 9 (56%) | 6 (37%) |
| Test 2 | 9 (56%) | 8 (50%) | 5 (31%) |
| Test 3 | 7 (44%) | 6 (37%) | 4 (25%) |
| Test 4 | 7 (44%) | 5 (31%) | 5 (31%) |
| Test 5 | 8 (50%) | 7 (44%) | 5 (31%) |
| Test 6 | 8 (50%) | 5 (31%) | 4 (25%) |
| Test 7 | 10 (62%) | 9 (56%) | 7 (44%) |
| Test 8 | 10 (62%) | 8 (50%) | 6 (37%) |
| Test 9 | 6 (37%) | 5 (31%) | 5 (31%) |
| Test 10 | 5 (31%) | 4 (25%) | 3 (19%) |

[a]Number of faults entirely located in areas of ΔCFS > 0 bar and percentage of total faults involved (total of 16 faults in all cases).

For paleoseismological earthquakes the location of the epicenters is unknown, and thus an earthquake may in fact have occurred in a part of the fault that was unloaded. Therefore, we also verified what happens if we restrict our tests just to the faults fully located in an area of $\Delta CFS_{cum} > 0$. Once all source faults that are partly in stress shadow are excluded, the actual sequence shows that ~ 56% of the faults are located in area of positive $\Delta CFS_{cum}$ for their entire length. Again, we were not able to reproduce the same percentages in the random tests, where the best result is 44% (and most of the other tests return 30% or less; see Table 4). From these tests it appears that our results are robust, and the time sequence and areal distribution of major earthquakes in this region in the last 1400 years is unlikely to be random.

### 5.3. Effect of Simplified Slip Distribution and Fault Geometry

In sections 3.3 and 3.4 we explained why our results are not really sensitive to the choice of rheological parameters in the model. The results, however, could in principle also be affected by oversimplifications due to lack of information concerning other parameters.

One possible issue is the slip distribution adopted for the source faults. We used a tapered slip distribution, which is different from reality, where the slip distribution is certainly more heterogeneous. The precise slip distribution, however, only affects the stress change pattern and values very close to the fault plane (a few kilometers), and it is therefore relevant only in main shock-aftershocks interaction studies and for earthquakes occurring on or near the source fault. Neither of these two conditions applies to our study; therefore, the assumption of a tapered slip distribution is a reasonable one.

The importance of fault geometry in ΔCFS calculations has already been explored by other works [e.g., *King et al*., 1994; *Madden et al*., 2013; *Wang et al*., 2014; *Verdecchia and Carena*, 2015]. In our particular case the main concern is linked to the dominant fault kinematics in this region, where many of the faults have a dominant or significant normal component, As mentioned earlier in section 3.2, due to lack of data on fault geometry at depth, we had to adopt a constant dip for the geometry of both source and receiver faults. Whereas this is not a problem for strike-slip faults, for which the dip most likely does not vary much with depth, it may not be the case for normal faults, which could have dip changes or a listric geometry still within the brittle crust. In order to assess the impact of using a simple planar geometry for normal faults, we compared the coseismic stress change pattern produced by a 60° dipping fault with the one produced by a fault with a dip of 60° for the top 5 km and 30° for the bottom 7 km (Figure S8). In both cases we kept the earthquake magnitude and average slip constant. The along-strike positive lobes (Figures S8a and S8b) appear to be slightly larger in the case of the more complex geometry. The maximum values of coseismic ΔCFS, however, do not change significantly. In addition, a localized positive stress change is created in the region where the fault dip changes (Figure S8f), but the effect is so local that it would be relevant only for analyzing the aftershocks distribution, which is not the subject of our work. Therefore, we opted for a high-angle, constant-dip geometry, which is also consistent with the few data on large historical earthquakes in the Basin and Range: the analyses of the 1954 Rainbow Mountain-Fairview Peak earthquakes [*Doser*, 1986], 1959 Hebgen Lake earthquake [*Doser*, 1985], and 1983 Borah Peak earthquake [*Stein and Barrientos*, 1985] all suggest a planar geometry of the source faults.

## 6. Conclusions

In order to better understand the relationships among large earthquakes in diffuse plate boundary regions, we modeled the evolution of coseismic and postseismic Coulomb stresses for 17 ground-rupturing earthquakes that occurred in the northern ECSZ, Walker Lane, and western Basin and Range in the last 1400 years.

Using geologic slip rates, we also determined the tectonic loading in the same period for all the major faults located in the study region.

Our results show that the majority of the source faults are partly or fully located in areas of positive stress loading produced by previous earthquakes. This indicates that the spatial distribution of major earthquakes in the region is controlled by coseismic and postseismic stress redistribution processes. In addition, the present-day sum of coseismic, postseismic, and interseismic stress change for the Fish Lake Valley Fault, Honey Lake Fault, Pyramid Lake Fault, Hunter Mountain Fault, White Mountain Fault, and Black Mountain Fault is comparable to the expected stress drop in a major earthquake. This finding suggests that these six faults may be close to failure at present, but, especially for the last three, further paleoseismological studies would be needed to confirm the absence of events younger than 1400 years.

**Acknowledgments**
The input file containing all our fault models and the file with geologic slip rates we used are both included as supporting information (Data Set S1 and Data Set S3). All the parameter values that we used are specified in this paper. We did neither collect nor produce any original data in our work: All the data we used have already been published by other authors, and the sources are listed in the references. We thank two anonymous reviewers for helping to improve the manuscript.

## References

Abbott, R. E., J. N. Louie, S. J. Caskey, and S. Pullammanappallil (2001), Geophysical confirmation of low-angle normal slip on the historically active Dixie Valley fault, Nevada, *J. Geophys. Res.*, *106*, 4169–4181, doi:10.1029/2000JB900385.

Ali, S. T., A. M. Freed, E. Calais, D. M. Manaker, and W. R. McCann (2008), Coulomb stress evolution in northeastern Caribbean over the past 250 years due to coseismic, postseismic and interseismic deformation, *Geophys. J. Int.*, *174*, 904–918, doi:10.1111/j.1365-246X.2008.03634.x.

Amos, C. B., S. J. Brownlee, D. H. Rood, G. B. Fisher, R. Bürgmann, P. R. Renne, and A. S. Jayko (2013), Chronology of tectonic, geomorphic, and volcanic interactions and the tempo of fault slip near Little Lake, California, *Geol. Soc. Am. Bull.*, *125*(7/8), 1187–1202, doi:10.1130/B30803.1.

Bassin, C., G. Laske, and G. Masters (2000), The current limits of resolution for surface wave tomography in North America, *Eos Trans. AGU*, *81*, F897.

Beanland, S., and M. M. Clark (1994), The Owens Valley fault zone, eastern California, and surface rupture associated with the 1872 earthquake, *U.S. Geol. Surv. Bull.*, *1892*, 1–32.

Bell, J. W., C. M. dePolo, A. R. Ramelli, A. M. Sarna-Wojcicki, and C. E. Meyer (1999), Surface faulting and paleoseismic history of the 1932 Cedar Mountain earthquake area, west-central Nevada, and implications for modern tectonics of the Walker Lane, *Geol. Soc. Am. Bull.*, *111*(6), 791–807.

Bell, J. W., S. J. Caskey, A. R. Ramelli, and L. Guerrieri (2004), Pattern and rates of faulting in the Central Nevada Seismic Belt, and paleoseismic evidence for prior beltlike behavior, *Bull. Seismol. Soc. Am.*, *94*, 1229–1254.

Bennett, R. A., B. P. Wernicke, N. A. Niemi, A. M. Friedrich, and J. L. Davis (2003), Contemporary strain rates in the northern Basin and Range province from GPS data, *Tectonics*, *22*(2), 1008, doi:10.1029/2001TC001355.

Bormann, J. M., B. E. Surpless, M. W. Caffee, and S. G. Wesnousky (2012), Holocene earthquakes and late Pleistocene slip rate estimates on the Wassuk Range fault zone, Nevada, USA, *Bull. Seismol. Soc. Am.*, *102*, 1884–1891, doi:10.1785/0120110287.

Briggs, R. W., and S. G. Wesnousky (2004), Late Pleistocene fault slip rate, earthquake occurrence, and recency of slip along the Pyramid Lake fault zone, northern Walker Lane, United States, *J. Geophys. Res.*, *109*, B08402, doi:10.1029/2003JB002717.

Caskey, S. J., and S. G. Wesnousky (1997), Static stress changes and earthquake triggering during the 1954 Fairview Peak and Dixie Valley earthquakes, central Nevada, *Bull. Seismol. Soc. Am.*, *87*, 521–527.

Caskey, S. J., S. G. Wesnousky, P. Zhang, and D. B. Slemmons (1996), Surface faulting of the 1954 Fairview Peak ($M_s$ 7.2) and Dixie Valley ($M_s$ 6.8) earthquakes, central Nevada, *Bull. Seismol. Soc. Am.*, *86*, 761–787.

Caskey, S. J., J. W. Bell, A. R. Ramelli, and S. G. Wesnousky (2004), Historic surface faulting and paleoseismicity in the area of the 1954 Rainbow Mountain-Stillwater earthquake sequence, central Nevada, *Bull. Seismol. Soc. Am.*, *94*, 1255–1275, doi:10.1785/012003012.

Chéry, J., S. Carretier, and J. F. Ritz (2001), Postseismic stress transfer explains time clustering of large earthquakes in Mongolia, *Earth Planet. Sci. Lett.*, *97*, 277–286.

Dawson, T. E., S. F. McGill, and T. K. Rockwell (2003), Irregular recurrence of paleoearthquakes along the central Garlock fault near El Paso Peaks, California, *J. Geophys. Res.*, *108*(B7), 2356, doi:10.1029/2001JB001744.

DeMets, C., R. G. Gordon, and D. F. Argus (2010), Geologically current plate motions, *Geophys. J. Int.*, *181*(1), 1–80, doi:10.1111/j.1365-246X.2009.04491.x.

Deng, J., and L. R. Sykes (1997), Evolution of the stress field in Southern California and triggering of moderate-size earthquakes: A 200-year perspective, *J. Geophys. Res.*, *102*, 9859–9886, doi:10.1029/96JB03897.

Dixon, T. H., E. Norabuena, and L. Hotaling (2003), Paleoseismology and Global Positioning System: Earthquake-cycle effects and geodetic versus geologic fault slip rates in the Eastern California Shear Zone, *Geology*, *31*, 55–58.

Dokka, R. K., and C. J. Travis (1990), Late Cenozoic strike-slip faulting in the Mojave Desert, California, *Tectonics*, *9*, 311–340, doi:10.1029/TC009i002p00311.

Doser, D. I. (1985), Source parameters and faulting processes of the 1959 Hebgen Lake, Montana earthquake sequence, *J. Geophys. Res.*, *90*, 4537–4556, doi:10.1029/JB090iB06p04537.

Doser, D. I. (1986), Earthquake processes in the Rainbow Mountain-Fairview Peak-Dixie Valley, Nevada, region 1954–1959, *J. Geophys. Res.*, *91*, 12,572–12,586, doi:10.1029/JB091iB12p12572.

Doser, D. I. (1988), Source parameters of earthquakes in the Nevada Seismic Zone, 1915–1943, *J. Geophys. Res.*, *93*, 15,001–15,015, doi:10.1029/JB093iB12p15001.

Field, E. H., et al. (2013), Uniform California earthquake rupture forecast, version 3 (UCERF3)—The time-independent model, *U. S. Geol. Surv. Open-File Rep. 2013–1165, Calif. Geol. Surv. Spec. Rep. 228, and South. Calif. Earthquake Cent. Publ. 1792*, 97 pp. [Available at http://pubs.usgs.gov/of/2013/1165/].

Frankel, K. L., J. F. Dolan, L. A. Owen, P. Ganev, and R. C. Finkel (2011), Spatial and temporal constancy of seismic strain release along an evolving segment of the Pacific-North America plate boundary, *Earth Planet. Sci. Lett.*, *304*, 565–576, doi:10.1016/j.epsl.2011.02.034.

Frankel, K. L., L. A. Owen, J. F. Dolan, J. R. Knott, Z. M. Lifton, R. C. Finkel, and T. Wasklewicz (2016), Timing and rates of Holocene normal faulting along the Black Mountains fault zone, Death Valley, USA, *Lithosphere*, *8*(1), 3–22, doi:10.1130/L464.1.

Freed, A. M. (2005), Earthquake triggering by static, dynamic and postseismic stress transfer, *Annu. Rev. Earth Planet. Sci.*, *33*, 335–367.
Freed, A. M., and R. Bürgmann (2004), Evidence of power-law flow in the Mojave Desert mantle, *Nature*, *430*, 548–551.
Freed, A. M., S. T. Ali, and R. Bürgmann (2007), Evolution of stress in Southern California for the past 200 years from coseismic, postseismic and interseismic stress changes, *Geophys. J. Int.*, *169*, 1164–1179, doi:10.1111/j.1365-246X.2007.03391.x.
Friedrich, A. M., B. P. Wernicke, N. A. Niemi, R. A. Bennett, and J. L. Davis (2003), Comparison of geodetic and geologic data from the Wasatch region, Utah, and implications for the spectral character of Earth deformation at periods of 10 to 10 million years, *J. Geophys. Res.*, *108*(B4), 2199, doi:10.1029/2001JB000682.
Gold, R. D., R. W. Briggs, S. F. Personius, A. J. Crone, S. A. Mahan, and S. J. Angster (2014), Latest Quaternary paleoseismology and evidence of distributed dextral shear along the Mohawk Valley fault zone, northern Walker Lane, California, *J. Geophys. Res. Solid Earth*, *119*, 5014–5032, doi:10.1002/2014JB010987.
Gourmelen, N., and F. Amelung (2005), Postseismic mantle relaxation in the Central Nevada Seismic Belt, *Science*, *310*, 1473–1476.
Haddon, E. K., C. B. Amos, O. Zielke, A. S. Jayko, and R. Bürgmann (2016), Surface slip during large Owens Valley earthquakes, *Geochem. Geophys. Geosyst.*, *17*, 2239–2269, doi:10.1002/2015GC006033.
Hammond, W. C., C. Kreemer, G. Blewitt, and H. P. Plag (2010), Effect of viscoelastic postseismic relaxation on estimates of interseismic crustal strain accumulation at Yucca Mountain, Nevada, *Geophys. Res. Lett.*, *37*, L06307, doi:10.1029/2010GL042795.
Hanks, T. C. (1977), Earthquake stress drops, ambient tectonic stresses and stresses that drive plate motion, *Pure Appl. Geophys.*, *115*, 441–458.
Harris, R. A., and R. W. Simpson (1998), Suppression of large earthquakes by stress shadows; a comparison of Coulomb and rate-and-state failure, *J. Geophys. Res.*, *103*, 19,835–19,858.
Hodgkinson, K. M., R. S. Stein, and G. C. P. King (1996), The 1954 Rainbow Mountain-Fairview Peak-Dixie Valley earthquakes: A triggered normal faulting sequence, *J. Geophys. Res.*, *101*, 25,459–25,471, doi:10.1029/96JB01302.
King, G. C. P., R. S. Stein, and J. Lin (1994), Static stress changes and the triggering of earthquakes, *Bull. Seismol. Soc. Am.*, *84*, 935–953.
Kirby, E., D. W. Burbank, M. C. Reheis, and F. Phillips (2006), Temporal variations in slip rate of the White Mountain Fault Zone, eastern California, *Earth Planet. Sci. Lett.*, *248*, 168–185, doi:10.1016/j.epsl.2006.05.026.
Klinger, R. E., and L. A. Piety (2001), Holocene faulting and slip rates along the Black Mountains fault zone near Mormon Point, in *Quaternary and Late Pliocene Geology of the Death Valley Region: Recent Observations and Tectonics, Stratigraphy, and Lake Cycles*, *U.S. Geol. Surv. Open File Rep. 01-51*, edited by M. N. Machette, M. L. Johnson, and J. L. Slate, pp. 245–270, U.S. Geol. Surv., Denver, Colo.
Lorenzo-Martín, F., F. Roth, and R. J. Wang (2006), Elastic and inelastic triggering of earthquakes in North Anatolian Fault zone, *Tectonophysics*, *424*, 271–289, doi:10.1016/j.tecto.2006.03.046.
Ma, K. F., C. H. Chan, and R. S. Stein (2005), Response of seismicity to Coulomb stress triggers and shadows of the 1999 $M_w$ = 7.6 Chi-Chi, Taiwan, earthquake, *J. Geophys. Res.*, *110*, B05S19, doi:10.1029/2004JB003389.
Machette, M. N., C. N. Martinez, A. J. Crone, K. M. Aller, and G. D'Addezio (1999), Geologic and seismic hazards investigations of the Cow Creek area, Death Valley National Park, California, *U.S. Geol. Surv. Open File Rep. 99-155*, 34 pp., Denver, Colo.
Madden, E. H., F. Maerten, and D. D. Pollard (2013), Mechanics of nonplanar faults at extensional steps with application to the 1992 *M* 7.3 Landers, California, earthquake, *J. Geophys. Res. Solid Earth*, *118*, 3249–3263, doi:10.1002/jgrb.50237.
Madugo, C. M., J. F. Dolan, and R. D. Hartleb (2012), New paleoearthquake ages from the western Garlock fault: Implications for regional earthquake occurrence in Southern California, *Bull. Seismol. Soc. Am.*, *102*, 2282–2299, doi:10.1785/0120110310.
Marsan, D. (2003), Triggering of seismicity at short timescales following Californian earthquakes, *J. Geophys. Res.*, *108*(B5), 2266, doi:10.1029/2002JB001946.
McAuliffe, L. J., J. F. Dolan, E. Kirby, C. Rollins, B. Haravitch, S. Alm, and T. M. Rittenour (2013), Paleoseismology of the southern Panamint Valley fault: Implications for regional earthquake occurrence and seismic hazard in Southern California, *J. Geophys. Res. Solid Earth*, *118*, 5126–5146, doi:10.1002/jgrb.50359.
Oskin, M., L. Peng, E. Shelef, M. Strane, E. Gurney, B. Singer, and X. Zhang (2008), Elevated shear zone loading during an earthquake cluster in eastern California, *Geology*, *36*(6), 507–510, doi:10.1130/G24814A.1.
Oswald, J. A., and S. G. Wesnousky (2002), Neotectonics and Quaternary geology of the Hunter Mountain fault zone and Saline Valley region, southeastern California, *Geomorphology*, *42*, 255–278.
Papadimitriou, E. E., and L. R. Sykes (2001), Evolution of the stress field in the northern Aegean Sea (Greece), *Geophys. J. Int.*, *146*, 747–759, doi:10.1046/j.0956-540x.2001.01486.x.
Parsons, T., S. Toda, R. S. Stein, A. Barka, and J. H. Dieterich (2000), Heightened odds of large earthquakes near Istanbul: An interaction-based probability calculation, *Science*, *288*, 661–665.
Peltzer, G., F. Crampe, S. Hensley, and P. Rosen (2001), Transient strain accumulation and fault interaction in the Eastern California Shear Zone, *Geology*, *29*(11), 975–978.
Petersen, M. D., W. A. Bryant, C. H. Cramer, T. Cao, N. S. Reichle, A. D. Frankel, J. J. Lienkaemper, P. A. McCrory, and D. P. Schwartz (1996), Probabilistic seismic hazard assessment for the state of California, *Calif. Div. of Mines and Geol. Open-File Rep. 96-08, U.S. Geol. Surv. Open File Rep. 96-706*, pp. 1–64.
Petersen, M. D., et al. (2014), Documentation for the 2014 update of the United States National Seismic Hazard Maps, *U. S. Geol. Surv. Open-File Rep. 2014–1091*, 243 pp., doi:10.3133/ofr20141091.
Pollitz, F. F. (2003), Transient rheology of the uppermost mantle beneath the Mojave Desert, California, *Earth Planet. Sci. Lett.*, *215*, 89–104.
Pollitz, F. F., M. Vergnolle and E. Calais (2003), Fault interaction and stress triggering of 20th century earthquakes in Mongolia, *J. Geophys. Res.*, *108*(B10), 2503, doi:10.1029/2002JB002375.
Ramelli, A. R., and J. W. Bell (2009), Spatial and temporal patterns of fault slip rates on the Genoa fault, NEHRP Final Tech. Rep., U.S. Geol. Surv., award G09AP00020.
Reheis, M. C. (1994), Logs of trenches across the central part of the Fish Lake Valley fault zone, Mono County, California, U.S. Geol. Surv. Misc. Field Stud. Map MF-2266, 20 pp., 1 plate.
Reheis, M. C., J. L. Slate, and T. L. Sawyer (1995), Geologic map of late Cenozoic deposits and faults in parts of the Mt. Barcroft, Piper Peak, and Soldier Pass 15′ quadrangles, Esmeralda County, Nevada, and Mono County, California, U.S. Geol. Surv. Misc. Invest. Map I-2464, 2 sheets.
Sarmiento, A. C., S. G. Wesnousky, and J. M. Bormann (2011), Paleoseismic trenches across the Sierra Nevada and Carson Range fronts in Antelope Valley, California, and Reno, Nevada, *Bull. Seismol. Soc. Am.*, *101*, 2542–2549, doi:10.1785/0120100176.
Savage, J. C. (1983), A dislocation model of strain accumulation and release at a subduction zone, *J. Geophys. Res.*, *88*, 4984–4996, doi:10.1029/JB088iB06p04984.
Sawyer, T. L., and M. C. Reheis (1999), Seismic potential of the Fish Lake Valley fault zone, Nevada and California, in *Proceedings of Conference on Status of Geologic Research and Mapping in Death Valley National Park, Las Vegas*, *U.S. Geol. Surv. Open File Rep. 99–153*, edited by J. L. Slate, pp. 132–140, U.S. Geol. Surv., Denver, Colo.

Scharer, K. M., G. P. Biasi, and R. J. Weldon II (2011), A reevaluation of the Pallet Creek earthquake chronology based on new AMS radiocarbon dates, San Andreas fault, California, *J. Geophys. Res.*, *116*, B12111, doi:10.1029/2010JB008099.
Scholz, C. H. (2002), *The Mechanism of Earthquake and Faulting*, 2nd ed., Cambridge Univ. Press, New York.
Scholz, C. H. (2010), Large earthquake triggering, clustering, and the synchronization of faults, *Bull. Seismol. Soc. Am.*, *100*, 901–909, doi:10.1785/0120090309.
Shan, B., X. Xiong, R. Wang, Y. Zheng, and S. Yang (2013), Coulomb stress evolution along Xianshuihe-Xiaojiang Fault System since 1713 and its interaction with Wenchuan earthquake, May 12, 2008, *Earth Planet. Sci. Lett.*, *377–378*, 199–210, doi:10.1016/j.epsl.2013.06.044.
Sohn, M. F., J. R. Knott, and S. A. Mahan (2014), Paleoseismology of the southern section of the Black Mountains and Southern Death Valley fault zones, Death Valley, United States, *Environ. Eng. Geosci.*, *20*, 177–198.
Stein, R. S. (1999), The role of stress transfer in earthquake occurrence, *Nature*, *402*, 605–609.
Stein, R. S., and S. E. Barrientos (1985), Planar high-angle faulting in the Basin and Range—Geodetic analysis of the 1983 Borah Peak, Idaho, earthquake, *J. Geophys. Res.*, *90*, 11,355–11,366, doi:10.1029/JB090iB13p11355.
Stein, R. S., G. C. P. King, and J. Lin (1994), Stress triggering of the 1994 $M = 6.7$ Northridge, California earthquake by its predecessors, *Science*, *258*, 1328–1332.
Stein, R. S., A. A. Barka, and J. H. Dieterich (1997), Progressive failure on the North Anatolian fault since 1939 by earthquake stress triggering, *Geophys. J. Int.*, *128*, 594–604.
Stein, S., and M. Liu (2009), Long aftershock sequences within continents and implications for earthquake hazard assessment, *Nature*, *462*, 87–89, doi:10.1038/nature085002.
Stewart, J. H. (1988), Tectonics and the Walker Lane Belt, western Great Basin: Mesozoic and Cenozoic deformation in a zone of shear, in *Metamorphism and Crustal Evolution of the Western United States, Rubey*, vol. VII, edited by W. G. Ernst, pp. 683–713 , Prentice-Hall, Old Tappan, N. J.
Surpless, B., and G. Kroeger (2015), The unusual temporal and spatial slip history of the Wassuk Range normal fault, western Nevada (USA): Implications for seismic hazard and Walker Lane deformation, *Geol. Soc. Am. Bull.*, *127*, 737–758, doi:10.1130/B31159.1.
Thatcher, W. (1995), Microplate versus continuum descriptions of active tectonic deformation, *J. Geophys. Res.*, *100*, 3885–3894, doi:10.1029/94JB03064.
Thatcher, W., and F. F. Pollitz (2008), Temporal evolution of continental lithospheric strength in actively deforming regions, *GSA Today*, *18*, 4–11, doi:10.1130/GSAT01804-5A.1.
Toda, S., J. Lin, M. Meghraoui, and R. S. Stein (2008), 12 May 2008 $M = 7.9$ Wenchuan, China, earthquake calculated to increase failure stress and seismicity rate on three major fault systems, *Geophys. Res. Lett.*, *35*, L17305, doi:10.1029/2008GL034903.
Toda, S., R. S. Stein, V. Sevilgen, and J. Lin (2011), Coulomb 3.3 graphic-rich deformation and stress change software for earthquake, tectonic, and volcano research and teaching—User guide, *U.S. Geol. Surv. Open-File Rep. 2011-1060*, 63 pp.
Turner, R., R. D. Koehler, R. W. Briggs, and S. G. Wesnousky (2008), Paleoseismic and slip-rate observations along the Honey Lake fault zone, northeastern California, U.S.A., *Bull. Seismol. Soc. Am.*, *98*, 1730–1736, doi:10.1785/0120070090.
Verdecchia, A., and S. Carena (2015), One hundred and fifty years of Coulomb stress history along the California-Nevada border, USA, *Tectonics*, *34*, 213–231, doi:10.1002/2014TC003746.
Wallace, R. E. (1984), Fault scarps formed during the earthquakes of October 2, 1915, in Pleasant Valley, Nevada, and some tectonic implications, in *Faulting Related to the 1915 Earthquakes in Pleasant Valley, Nevada*, *U.S. Geol. Surv. Prof. Pap. 1274-A*, pp. A1–A33, U.S. Gov. Print. Off., Wash.
Wallace, R. E. (1987), Grouping and migration of surface faulting and variations in slip rates on faults in the Great Basin province, *Bull. Seismol. Soc. Am.*, *77*, 868–876.
Wang, J., C. Xu, J. T. Freymueller, Z. Li, and W. Shen (2014), Sensitivity of Coulomb stress change to the parameters of the Coulomb failure model: A case study using the 2008 $M_w$ 7.9 Wenchuan earthquake, *J. Geophys. Res. Solid Earth*, *119*, 3371–3392, doi:10.1002/2012JB009860.
Wang, R., F. Lorenzo-Martín, and F. Roth (2006), PSGRN/PSCMP – A new code for calculating co- and post-sesimic deformation, geoid and gravity changes based on the viscoelastic-gravitational dislocation theory, *Comput. Geosci.*, *32*, 527–541.
Wells, D. L., and K. J. Coppersmith (1994), New empirical relationship among magnitude, rupture length, rupture width, rupture area, and surface displacement, *Bull. Seismol. Soc. Am.*, *84*, 974–1002.
Wesnousky, S. G. (2005), Active faulting in the Walker Lane, *Tectonics*, *24*, TC3009, doi:10.1029/2004TC001645.
Wesnousky, S. G., J. M. Bormann, C. Kreemer, W. C. Hammond, and J. N. Brune (2012), Neotectonics, geodesy, and seismic hazard in the northern Walker Lane of western North America: Thirty kilometers of crustal shear and no strike-slip?, *Earth Planet. Sci. Lett.*, *329–330*, 133–140, doi:10.1016/j.epsl.2012.02.018.